ALMA MATER STUDIORUM – UNIVERSITÀ DI BOLOGNA

SECONDA FACOLTÀ DI INGEGNERIA CON SEDE A CESENA
CORSO DI LAUREA MAGISTRALE IN INGEGNERIA AEROSPAZIALE

Sede di Forlì
Classe LM-20

NUMERICAL INVESTIGATION OF TURBULENT/NON-TURBULENT INTERFACE

Tesi in
COMPLEMENTI DI FLUIDODINAMICA LM

Relatore:
Prof. ELISABETTA DE ANGELIS

Presentata da:
GIACOMO COCCONI

Correlatore:
Dott. ANDREA CIMARELLI

Sessione III
Anno Accademico 2011/2012

Contents

Introduction

The subject of this work is the diffusion of turbulence in a non-turbulent flow. Such phenomenon can be found in almost every practical case of turbulent flow: all types of shear flows (wakes, jet, boundary layers) present some boundary between turbulence and the non-turbulent surround; all transients from a laminar flow to turbulence must account for turbulent diffusion; mixing of flows often involve the injection of a turbulent solution in a non-turbulent fluid.

The mechanism of what Phillips defined as *"the erosion by turbulence of the underlying non-turbulent flow"*, is called entrainment. It is usually considered to operate on two scales with different mechanics. The small scale nibbling, which is the entrainment of fluid by viscous diffusion of turbulence, and the large scale engulfment, which entraps large volume of flow to be "digested" subsequently by viscous diffusion. The exact role of each of them in the overall entrainment rate is still not well understood, as it is the interplay between these two mechanics of diffusion. It is anyway accepted that the entrainment rate scales with large properties of the flow (Tsinober 2001, Westerweel et al 2009), while is not understood how the large scale inertial behavior can affect an intrinsically viscous phenomenon as diffusion of vorticity.

In the present work we will address then the problem of turbulent diffusion through pseudo-spectral DNS simulations of the interface between a volume of decaying turbulence and quiescent flow. Such simulations will give us first hand measures of velocity, vorticity and strains fields at the interface; moreover the framework of unforced decaying turbulence will permit to study both spatial and temporal evolution of such fields.

The analysis will evidence that for this kind of flows the overall production of enstrophy , i.e. the square of vorticity ω^2, is dominated near the interface by the local inertial transport of "fresh vorticity" coming from the turbulent flow. Viscous diffusion instead plays a major role in enstrophy production in the outbound of the interface, where the nibbling process is

dominant. The data from our simulation seems to confirm the theory of an inertially stirred viscous phenomenon proposed by others authors before and provides new data about the inertial diffusion of turbulence across the interface.

Chapter 1

Turbulent/non-turbulent interface

1.1 An overview on the turbulence problem

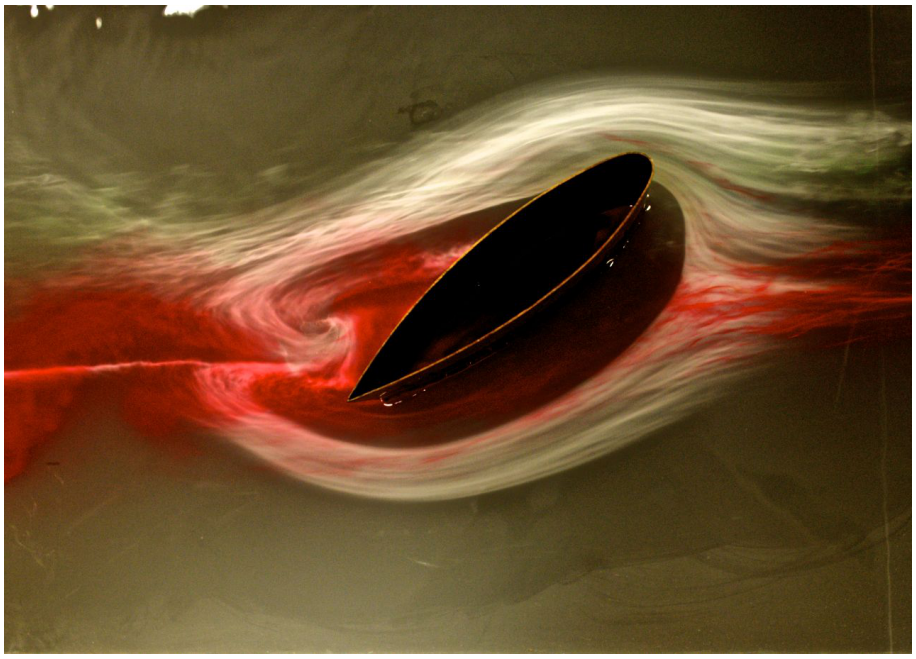

Turbulence is an omnipresent phenomenon and can be commonly experienced almost any time we are in presence of the motion of a fluid: the airflow around an airfoil, the mixing of air and gasoline in engines, the blood moving through the vessels, the atmospheric turbulence or the magneto-hydrodynamic flows in the earth core are few examples of phenomena governed by turbulence. As these examples shows, it is a subjects which affects a

huge range of science branches and engineering applications.
Since the very first days of the fluid-dynamics science, turbulence had been the main obstacle to a mathematical description of the motion of fluids behavior. A famous quote attributed to Heisenberg says: *"When I meet God, I am going to ask him two questions: Why relativity ? And why turbulence ? I really believe he will have an answer for the first"*, Feynman defined turbulence as *""the most important unsolved problem of classical physics",* von Neumann noted in a 1949 review of turbulence that *"... a considerable mathematical effort towards a detailed understanding of the mechanism of turbulence is called for"* but that, given the analytic difficulties presented by the turbulence problem, *"... there might be some hope to 'break the deadlock' by extensive, but well-planned, computational efforts."*. The study of turbulence has made progress since then but, despite the efforts of some of the greatest minds in modern science, a full physical comprehension of many of its aspect seems still far. Perhaps the best summary of the difficulties encountered dealing with turbulence is given by Kraichnan (1972): "*Turbulent flow constitutes an unusual and difficult problem of statistical mechanics, characterized by extreme statistical disequilibrium, by anomalous transport processes, by strong dynamical nonlinearity, and by perplexing interplay of chaos and order*"
Turbulence, respect to a laminar flow, brings a significant increase of diffusion rates of momentum and scalar passive (hence temperature, suspended particles, solutes). A simple example can show how such rates of diffusion are incredibly greater then the molecular equivalent: if we consider the diffusion of a cigarette smoke and we hypothesize a purely molecular diffusion, the time scale of diffusion is of the order of $T = L^2/k$ (k is the diffusivity of smoke in air). With $k = \nu/Sc$, a Scmidth number Sc of about 0.7 for the air, a kinematic viscosity in the order of 10^{-5} ($kg/m \cdot s$) the smoke would take about 8 days to diffuse in the room, while the actual time scale thanks to turbulence is in the order of few seconds.
Some characteristic of turbulence, as the increased diffusion rates, are something desirable in some application, e.g. mixing of chemicals or heat exchangers. In some applications on the other hand, is something that must be avoided or precisely accounted for, e.g. friction reduction or ablative thermal shielding.
Should not surprise then the amount of studies that can be found on the matter, many of which are dedicated to extremely specialized and rare manifestations of turbulence. The literature on turbulence is equally vast and will be only briefly addressed further in the

reading.
The core subject of this thesis is the diffusion of turbulence when it coexist with non-turbulent fluid; despite it is a condition which can be found in almost every turbulence problem, it is still a non trivial phenomenon. For example it is accepted that the only mechanism of diffusion of turbulence in irrotational fluid is through viscous interactions, yet it seem to be Reynolds independent and it scales with big scales properties of the flow (see Townsend 1956). The literature on the subject is vast but both experimental and numerical analysis did until the last ten years lacked an accurate analysis on the evolution of the vorticity fields (due to technology constraints); especially the formers used to concentrate on turbulence related quantities such the intermittency (Corrsin and Kistler 1955) which can be sometimes misleading. The recent development of PIV technology on the experimental side and the growth of computational power on the other, boosted a new wave of studies on the subject which eventually comprehended extensive study of both vorticity and strain fields (see Westerweel 2002, Liberzon 2005, Holzner 2006). In the first part of the thesis some of the results of these works will be addressed, briefly preceded by the strictly necessary theoretical framework on turbulence and turbulent interface. Will follow the results from the two different simulations carried out for this research: first the simulation of a an interface with decaying homogeneous isotropic turbulence without mean shear, second the study of the temporal evolution of the interface between a jet an its irrotational surround.
The interface with decaying turbulence can be thought as one of the most simplified cases: here a box of initially homogeneous isotropic turbulence is put beside an equivalent box of quiescent flow, a smoothing function provides the contact area between the two boxes with an initial artificial interface. The turbulence can then freely evolve and diffuse in the non-turbulent box.
The absence of any external forcing permit to reduce to the minimum the number of the parameters which can affect the interface behavior and focus exclusively on diffusion mechanics.

1.2 Equations of fluid mechanics

In this section some basic results of fluid-dynamics will be briefly revised, these will be necessary to better understand some specific terms analyzed in this work. Furthermore it

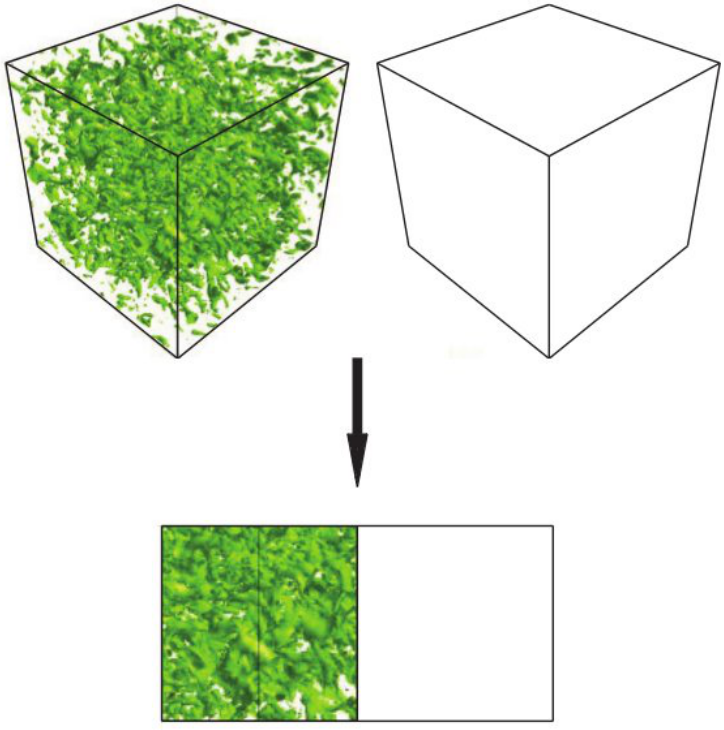

Figure 1.1.1: Set-up of the interface experiment: a triperiodic box of homogeneous isotropic turbulence is put beside an equal box of static flow and then let freely evolve.

will show the notation used throughout the work.
The two main approaches used to describe fluids motion are the *Lagrangian* and the *Eulerian* representations. The Lagrangian description considers the dynamic of fluid particles, i.e., a point which have the local velocity of fluid; thus it describes the trajectories of a specific fluid particles. The position at a given time of a particle is denoted as $\mathbf{X}^+(\mathbf{Y}, t)$, where $\mathbf{Y}$ is the position of the particle at a fixed reference time t_0; Lagrangian field are in this way indexed by the material coordinate $\mathbf{Y}$. For example a velocity field is defined as

$$\frac{\partial}{\partial t}\mathbf{X}^+(\mathbf{Y}, t) = \mathbf{U}(\mathbf{X}^+(\mathbf{Y}, t), t) \equiv \mathbf{U}^+(\mathbf{Y}, t) \tag{1.2.1}$$

The Eulerian representation on the other hand, consider only variations of continuous fluid properties at fixed positions, through which the fluid particles moves.
The rates of change in the Lagrangian representations is usually called *material* or *substantial derivative,* which relate to the partial derivative in the Eulerian description as

$$\frac{D}{Dt} \equiv \frac{\partial}{\partial t} + U_i\frac{\partial}{\partial x_i} = \frac{\partial}{\partial t} + \mathbf{U} \cdot \nabla \tag{1.2.2}$$

The Eulerian representation is often preferred for its ease of use, anyway some physical aspect shown further in the reading will require a Lagrangian description. Moreover Lagrangian representation is useful to investigate small scales behaviors in turbulence, as did in Holzner (2007) just to cite an example related to the thesis subject.

1.2.1 Mass and momentum conservation

Mass conservation or continuity equation is given by

$$\frac{\partial \rho}{\partial t} + \nabla \cdot (\rho \mathbf{u}) = 0 \tag{1.2.3}$$

or

$$\frac{\partial \rho}{\partial t} + \rho \nabla \cdot \mathbf{u} + \mathbf{u} \cdot \nabla \rho = 0 \tag{1.2.4}$$

in incompressible flows ρ is constant, the only other equation is then the one which grant a *solenoidal* velocity field or

$$\nabla \cdot \mathbf{u} = 0 \quad or \quad \frac{\partial u_i}{\partial x_i} = 0 \tag{1.2.5}$$

In this work compressibility can be safely neglected due to the low velocity and relatively low gradients experienced in the numerical experiments that will be treated.
The momentum equation relates the acceleration of the fluid particle to all the forces applied to it, this lead to the *Navier-Stokes equations*:

$$\frac{\partial \mathbf{u}}{\partial t} + (\mathbf{u} \cdot \nabla)\mathbf{u} = -\frac{\mathbf{1}}{\rho}\nabla \mathbf{p} + \mathbf{f} + \nu \nabla^{\mathbf{2}}\mathbf{u} \tag{1.2.6}$$

or in Einstein notation

$$\frac{\partial u_i}{\partial t} + u_j \frac{\partial u_i}{\partial x_j} = -\frac{1}{\rho}\frac{\partial p}{\partial x_i} + f_i + \nu \frac{\partial^2 u_i}{\partial x_i^2} \tag{1.2.7}$$

Tanks to incompressible hypothesis, taking the divergence of the last equation leads to the equation

$$\nabla^2 p = -\nabla \cdot [(\mathbf{u} \cdot \nabla)\,\mathbf{u}] \tag{1.2.8}$$

hence, for incompressible flows, pressure is not related with density and temperature by an equation of state as usual; it is uniquely determined by the velocity field. Moreover the pressure appears only through its gradient only, hence constant pressure doesn't affect directly the momentum equation.

1.2.2 Homogeneous isotropic turbulence

For the simulation of the interface a box of homogeneous isotropic turbulence will be used as initial condition. Homogeneous turbulence means that the flow is statistically invariant to translations of the reference system, which means that the statistics of a certain flow property are the same in any point of the domain (there are no spatial gradients in any averaged quantity). Isotropy on the other hand brings invariance to rotations and reflections of the reference system, hence statistical invariance to the direction.
These simplifying assumptions mean that equation of turbulence comes without all the terms related to mean velocity fields. Furthermore it is a condition which has been extensively studied and for which are available a number of consolidated theoretical and

experimental results. Kolmogorov turbulence theory provides predictions for the energy spectra of such flows and is used as starting point by many other theories. Moreover his hypothesis of local isotropy states that for large enough Reynolds numbers and for small enough regions of the space, homogeneity and isotropy are found even in non-isotropic flows.

Departures from theoretical results can be then easily attributed to the mechanics of turbulent/non-turbulent interface. While is a condition never actually encountered in real flows, a good experimental approximation of isotropic homogeneous turbulence can be obtained with grids in wind tunnels where isotropy is reached at some diameters from the grid; must noted that grid turbulence in wind-tunnels is close to homogeneity except for the persistence of pressure transport and transverse energy transport (see Valente and Vassilicos 2011).

In wind tunnels grid turbulence the decay of turbulence can be statistically studied probing the flow at increasing distances from the grid (although this imply the use of Taylor's frozen turbulence approximation). In homogeneous isotropic turbulence the decay of kinetic energy can be theoretically estimated by means of the equation for the kinetic energy variation

$$\frac{\partial E}{\partial t} + \nabla \cdot (\mathbf{u}(p+E)) = -\nu \mathbf{u} \cdot \nabla \times \omega \tag{1.2.9}$$

or

$$\frac{\partial E}{\partial t} + \nabla \cdot (\mathbf{u}\,(p+E) + \nu\omega \times \mathbf{u}) = -\nu\omega \cdot \omega. \tag{1.2.10}$$

The flux term when averaged vanish leaving the relation for the dissipation

$$\frac{\partial \langle E \rangle}{\partial t} = -\epsilon \tag{1.2.11}$$

where

$$\epsilon = 2\nu \left\langle \frac{\omega^2}{2} \right\rangle \tag{1.2.12}$$

The former relation shows how variations in turbulent kinetic energy E, in a statistically steady flow, are balanced by viscous dissipation ϵ. Equation 1.2.12 illustrate how strictly related are dissipation and enstrophy in homogeneous isotropic turbulence.

Is useful to consider now the spectral version of the kinetic energy equation, the resolution of the Navier-Stokes equations in Fourier space will not be discussed here as it is long and can be easily found in a number of textbook. In the Fourier space for a given wave number k, with

$$k = \frac{2\pi}{\lambda}, \tag{1.2.13}$$

(λ is the wavelength) the relation for the variation of kinetic energy becomes

$$\frac{\partial}{\partial t}E(k,t) = T(k,t) + F(k,t) - 2\nu k^2 E(k,t), \tag{1.2.14}$$

where $T(k,t)$ is the kinetic energy transfer due to non-linear interaction, $F(k,t)$ is the term of forcing, and $-2\nu k^2 E(k,t)$ is the dissipation.

Now the Kolmogorov first similarity hypothesis states hat for the locally isotropic turbulence the energy spectrum distribution is uniquely determined by the dissipation ϵ and the viscosity ν.

The second similarity hypothesis states that, if the separation between the energy injecting scale and the dissipation scale η is large enough, in the range between these two scales (the inertial range) the energy spectrum is uniquely determined by ϵ and does not depend on ν.

Starting from this last hypothesis, the dimensional analysis leads for the inertial range to a energy spectrum which decades as

$$E(k) = C_k \cdot \langle\epsilon\rangle^{\frac{2}{3}} k^{-\frac{5}{3}}, \tag{1.2.15}$$

where C_k is an universal constant.

There are a series of issues on Kolmogorov theory, first of all the validity of local isotropy assumption. A number of studies have reported some departures for high order statistics from isotropy in high Reynolds numbers shear flows (Tsinober 2001). Such flows seems to preserve in the inertial range some memory of the forcing scales meaning that the energy cascade is not an information losing process. This is only the case for flow with large scale anisotropy and high Reynolds numbers but even isotropic homogeneous turbulence seems to preserve some dependence from large scale parameters down to the dissipative range. George (1992) demonstrated the possibility of the existence of solutions to the averaged spectral equations that are both self-preserving at all scales of motion and dependent to the

initial conditions.
For decaying homogeneous isotropic turbulence, the length of validity of the similarity hypothesis is the Taylor microscale λ and the energy variation in time is related to λ by

$$E(t) \sim u^2 \lambda \tag{1.2.16}$$

(see George 1990) and decay of the kinetic energy undergoes to a power law

$$u^2 \sim t^n \tag{1.2.17}$$

The dissipation can be related to both kinetic energy and Taylor microscale through

$$\epsilon = 15\nu \frac{u^2}{\lambda^2}. \tag{1.2.18}$$

or either related to the integral scale through

$$\epsilon \sim \frac{u'^3}{L} = \frac{E^{\frac{3}{2}}}{L} \tag{1.2.19}$$

where u' is the r.m.s. of velocity fluctuations.
According to Von Kármán result the Taylor microscale increases as the square root of time, or

$$\lambda = \sqrt{-\frac{10}{n}\nu t} \tag{1.2.20}$$

thus

$$\frac{d\lambda^2}{dt} = -\frac{10}{n} \tag{1.2.21}$$

The linear growth of λ^2 for decay turbulence has shown to fit with actual data in grid-induced turbulence quite well as proven for example by Comte-Bellot and Corrsin (1966). Grid turbulence has demonstrated as well a strong dependence on initial conditions of decay laws, Warhaft and Lumley (1978) in their study on heated grids found strong variations of temperature fluctuations decay rate depending on the initial temperature.
About the actual value of n there are multiple results depending on some characteristic of the flow. For virtually infinite initial Reynolds number the Von Kármán-Howart solution predict a decay rate of t^{-1}, instead for finite initial Reynolds number most experiment

reports $n < -1$ (Comte-Bellot and Corrsin 1971 , Wray 1998, Wang and George 2003). The power law of decay with various values for the exponent n has proven to fit well both data from grid induced turbulence and DNS but recent experiment with fractal grids (Seud and Vassilicos 2007 and Valente and Vassilicos 2011) found the decay rate to be governed by an exponential law rather then a power law. Being

$$\frac{dE}{dt} = -10\nu\frac{E}{\lambda^2}, \tag{1.2.22}$$

a power law is possible only if the Taylor microscale remain constant during decay, so that the time derivative of the kinetic energy is proportional to the kinetic energy (George 2013). George and Wang (2009) shown that both decay laws are consistent with an equilibrium similarity analysis of the spectral energy equations, yet is not well understood what drives the flow to a decay law rather than the other.

1.3 Turbulent/non-turbulent interface

1.3.1 The entrainment

As mentioned in the introduction turbulence is a complex phenomenon, so some basic physical aspect of this problem must be addressed before a further insight in the subject of turbulent/non-turbulent interface.
Turbulence cover such a range of yet not understood flow behaviors that a comprehensive definition for it has not found at the time. Despite the attempts of many to found an universal definition for it, the best way to define turbulence is still by a list of its properties. Turbulent flow are expected to show:

- Intrinsic randomness in space and time variations. This feature arise form the extreme sensibility to disturbance of the Navier-Stokes equations, which lead such deterministic equations to a chaotic behavior.

- An extremely wide range of scales strongly interacting together. The interaction between the many degrees of freedom results from the non-linearity of turbulent flows.

- Loss of predictability, different realizations starting from apparently identical initial

conditions leads to much different results. Nevertheless, different realizations of the same turbulent flow shares the same statistical properties; thus turbulent flows posses both predictable an unpredictable features.

- High dissipation; turbulence require energy in order to be maintained. The energy supply is mostly at large scales while dissipation occurs at small ones.
- Three-dimensions and rotational field, even if there's still a debate about the existence of 2D turbulence.
- Strong diffusion; transport processes of momentum and passive objects are enhanced.

Aside the qualitative definition of turbulence there are some quantitative features which can be used in order to identify the onset of turbulence (e.g. vorticity thresholds), though such features depends on the flow characteristics and lacks the universality of the aforementioned definition. Some of these quantitative features will be shown further in the work as will arise the need for a detection algorithm of the turbulent interface.
In most bounded flows and in all practical cases of unbounded flows, turbulence coexists with regions of irrotational flow: boundary layers, jet, wakes, plumes, mixing layers (basically all the free shear turbulence) are examples that show how vast is this category of phenomena. The interface between the turbulent flow and the surrounding inviscid irrotational flow appears highly irregular and convoluted, its shape and position ever changing. The first attempt of dealing with such physical problem has been through the definition of the *intermittency* γ (Corrsin and Kistler 1955), which is the fraction of time in which a fixed point of measurement experience a turbulent flow. Such ratio has been derived directly from the first hot-wire velocity measurement in the regions at the boundaries of turbulent flows, where the probes experience strong fluctuations for small time intervals.
With a process called *entrainment* non-turbulent fluid, due to the action of neighboring rotational flow, acquires vorticity, and become part of the turbulent mass; thus the region affected by turbulence tend to spread. The onset of vorticity in irrotational flow is exclusively determined by viscous interactions with turbulent eddies in the interface area, there is therefore a strong relation between entrainment and dissipation.
Using the definition given by Phillips (1966) the entrainment is "*the erosion by turbulence of the underlying non-turbulent flow*". Entrainment is a process which concerns also laminar flow, for example in the extent that a jet draws fluid from the sides and confer

kinetic energy to it; even in the laminar case the entrainment can be related to the energy dissipation.
Entrainment has a central role in mixing properties as transport rates of momentum and vorticity as well as passive quantities like temperature or concentration of suspended phases; thus the the problem of modeling the behavior of the spreading of turbulence in an irrotational fluid had been at the center of many studies in the past years.
The entrainment is usually thought to act both at large and small scales with different mechanics. Viscous , i.e. small scale, interactions act diffusing into non-turbulent region and converting non-turbulent fluid in turbulent. This interactions generate small structures of rotational flow which protrude toward the irrotational fluid originating the so called nibbling.

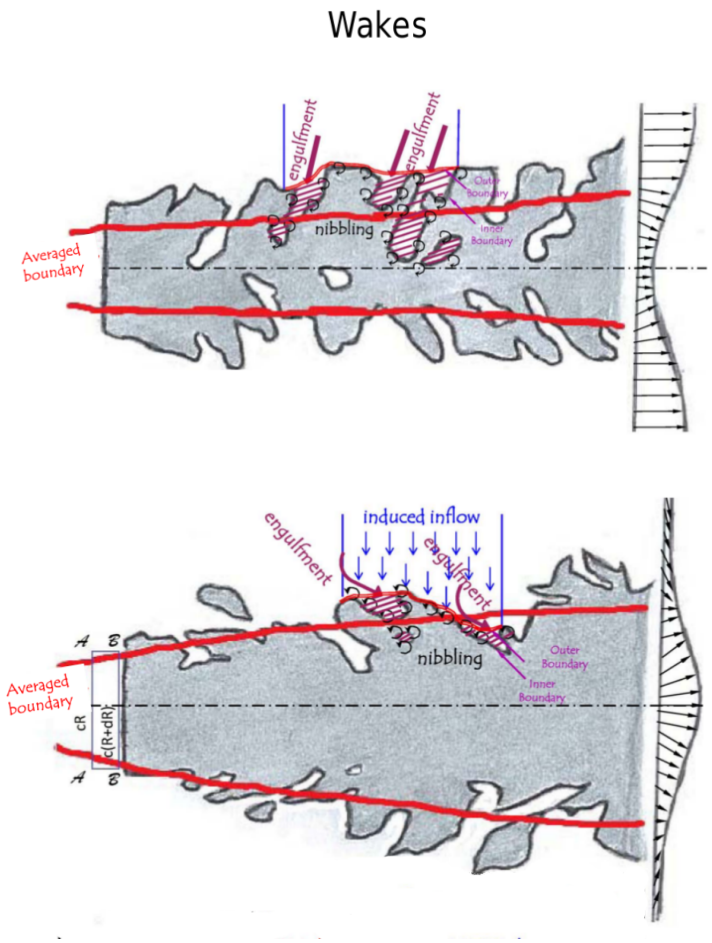

Figure 1.3.1: Nibbling and engulfment in a wake and in a jet (from Philip 2012)

At large scales engulfment entrap large zones of non-turbulent flow which is successively "digested" by small scale nibbling. Moreover large scale fluctuations act by increasing the surface area of the interface, thus the area affected by turbulence diffusion.
Philip classified three type of entraining flows, differentiating them on the base of the characteristic of their entrainment process. He stated that there are differences between grid induced turbulence, jets interfaces, wakes and boundary layers interfaces. Jet flows for example are characterized by an induced inflow of fluid which cannot be found for example in wakes and boundary layers. Hence the differences between engulfment contribute estimates in various studies may be probably explained by intrinsically different entrainment dynamics.
The relative weight in the entraining process of engulfing and nibbling has been at the center of many studies on turbulent interfaces, nevertheless since today the interplay between the two mechanism of entrainment has not permitted yet to find which is the predominant in turbulence diffusion.

1.3.2 Interface detection

The interface can defined as the thin layer across which the flow is found turbulent, i.e acquire all the properties listed the previous section. It is a convoluted unsteady surface, whit strong fluctuations of velocity and vorticity (as the idea itself of describing it through intermittency may suggests). The surface of the interface is actually hard to identify, in fact the flow in proximity of the interface is characterized by inclusions of laminar flow and bubbles of vorticity in the irrotational field which evolve continuously.
The study of partially turbulent flows pose again the problem of defining what is turbulence. The qualitative description given in the previous chapter can clearly discern in these kind of flows turbulent areas from the non-turbulent ones; the question is now how can be said whether a small part of the flow is turbulent or not.
A criterion to define locally when a part of the flow is turbulent must be found before proceeding in the study of turbulent interface. Most of the criteria used until now imply taking some arbitrary level of a flow quantity as marker of the inset of turbulence. Corrsin (1943) and Kistler (1954, 1955) used first the distinction in rotational turbulent region and the almost potential non-turbulent ones as discriminating criterion. Such distinction offer a quantitative mean of detecting the interface between turbulent and laminar flow but it

had been difficult to implement practically until now-days, since it requires information on vorticity.

The development of PIV permitted in the last years to measure vorticity fields in small control volumes, yet the accuracy of such measurements is poor for detection purpose and the measure of the vorticity is often used beside some other detection technique (as in Westerweel et al 2005, Holzner et al. 2006) . DNS on the other hand give access to the full velocity field data and application of a vorticity threshold as detection method confirmed itself as a valid approach; Bisset et al. (1998, 2001) as well as Holzner (2006) found a steep change in vorticity across the turbulent/non-turbulent interface.

Holzner et al (2006, 2007) gives an exhaustive analysis of a series of experimental and numerical interface detection techniques in a water-filled tank with grid-induced turbulence; among them is described the combined use of particle image velocimetry (PIV) and planar laser-induced fluorescence before used by Westerweel (2002). Here a fluorescent dye, with low Schmidt numbers, is injected in the turbulent part of the flow where it rapidly diffuse. The low Schmidt number ensure that the molecular diffusion is negligible respect turbulent mixing. A planar cross section of the test chamber is then illuminated by an intermittent laser sheet, two different camera capture the same image of the flow in rapid succession in such a way to obtain a normal and an illuminated caption of the flow at almost the same instant. The former caption will give the data for the PIV and the latter will show the which part of the velocity field is interested by the dye, i.e. the turbulence. With such technique the smallest scales of the dye concentration field are of the order of the Batchelor scale (Holzner et al. 2006), defined as

$$\eta_B = \frac{\eta}{\sqrt{Sc}} \tag{1.3.1}$$

Holzner with such method reported a smallest scale for the concentration field one order of magnitude smaller then the smallest resolved scale. This technique has also the merit to give access to the full instantaneous field of the vorticity component normal to the laser sheet plane, which has been used in order to study the enstrophy production near the interface. The thresholds technique have been proven before against the tracking of some passive scalar or dye (as in Westerweel et al. 2009 and Holzner et al. 2006), anyway both techniques tend to overestimate the position of the interface H(t) (in Holzner et al. 2006 is reported an evaluation of such errors).

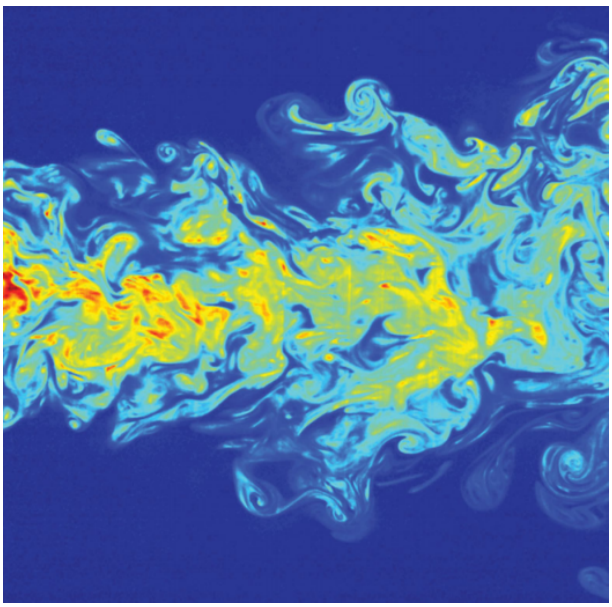

Figure 1.3.2: Concentration field of dye in turbulent jet (Westerweel 2009)

Non-rotational fluid can acquire a non-zero vorticity only by means of molecular viscous diffusion through the interface with the turbulent flow, thus the main mechanism of turbulent diffusion is expected to be related with small viscous scales; this is the main reason why the width of the interface across which the vorticity rise to turbulent-side's levels is comparable to the scales of viscosity. As observed in experiments the thickness of the interface is of the order of the Taylor microscale ($\sim L_x/Re^{1/2}$) (Westerweel 2009), but in the absence of a strong shear the thickness may reduce to the Kolmogorov scale ($\sim L_x/Re^{3/4}$) (Holzner et al. 2007, 2008). As noted before, Corrsin and Kistler (1954) used first the vorticity as quantitative detection technique, due to the sharpness in the separation between rotational turbulent flow and irrotational flow. Other quantities present a similar behavior across the interface, among them velocity fluctuation thresholds have been tested by both Bisset et al. (2002) and Westerweel et al. (2002). A thresholds discriminant must be imposed due to the velocity fluctuations induced by the interface in the non-turbulent region, nevertheless these decay rapidly with the distance from the interface.

Vorticity alone is not a sufficient condition to define locally a fluid as turbulent, experiments must take in account for the random nature of the flow in both sides of the interface and some trace of vorticity can be found in the non-turbulent side. This virtually imply another mechanism of entrainment: weakly turbulent seeds in the irrotational part of the

flow may be entrained due to the vortex stretching mechanism as pointed out by Tsinober " an initially Gaussian and *potential* velocity field with small seeding of vorticity will produce - at least for a short time - an essential positive enstrophy (as well as production of strain) though strictly this is true for homogeneous turbulence" although as stated in Bisset et al. (1998, 2001) such mechanism can be effective only in the proximity of the interface where large strain should exist (fluctuations attenuate exponentially with the distance from the turbulent interface).
Beside the randomness of the flow considered above, the non turbulent side of the field is found to be subject to non-rotational velocity fluctuations induced by the movements of the interface itself. Phillips (1955) studied with a theoretical approach the energy of such fluctuations at an increasing distance r_i from the interface. At sufficient distances the irrotational field can be described by a potential Φ, setting $\nabla\Phi = 0$ at $r_i \to \infty$ and a random distribution of normal velocity at the interface, he predicted a decay for the average square root of the velocity fluctuation energy $\langle v \rangle \propto r_i^{-2}$. Despite the coarse assumption for the interface, the prediction had been proved to hold in a boundary layer experiment by Bradshaw (1967) yet only at several boundary layer thickness away from the interface.
Recently Borrell and Jiménez questioned the capability of the threshold approach to grasp the characteristics of the interface: according to them the variation of the threshold strongly affect the topology of the interface detected and obviously its detected position.

1.3.3 Entrainment rate

As mentioned before entrainment is essentially a viscous (small scale) process, yet experimental evidence (Tritton 1988; Tsinober 2001; Hunt, Eames and Westerweel 2006) had shown that turbulence diffusion scale with the bigger scales of the flow. At large Reynolds number the entrainment rate and the propagation velocity of the interface (relative to the fluid flow) become independent to viscosity (Townsend 1976, Bisset et al. 2001). Hence the overall rate of entrainment is set by large-scale parameters of the flow while the actual spreading is brought about by the viscosity (Tritton 1988). As clearly stated by Tsinober "small scales do the 'work', but the amount of work is fixed by large scales in such a way that the outcome is independent of viscosity". The slow diffusion of viscosity into the irrotational fluid must be accelerated by the interaction of velocity fields of eddies of all sizes, in such a way that the overall rate of entrainment is set by large scale parameters of

the flow (Holzner et al. 2007).
About the entrainment rate, two different characteristic velocity can be defined: *entrainment velocity* u_a and *propagation velocity* v_e (as seen in Liberzon et al. 2009). The former is the velocity of the fluid relative to the turbulent/non-turbulent interface. In their Lagrangian analysis of grid-generated turbuelnce, Holzner et al. (2007) found that locally a particle cross the interface with a velocity which scale with the Kolmogorov velocity $u_\eta = (\epsilon\nu)^{\frac{1}{4}}$, which substantially confirm the small scale nature of the onset of entrainment. The advancement of the mean position $H\,(t)$ of the interface toward the non-turbulent region gives instead the propagation velocity $v_e = dH/dt$. Phillips (1972) related v_e and u_a through the geometry of the interface $\zeta(y, z, t)$ (which location has been found with the threshold technique) with the equation

$$v_e = u_a \left\langle 1 + (\nabla\zeta)^2 \right\rangle^{\frac{1}{2}} \tag{1.3.2}$$

where the average refer the plane $y - z$. In the case of turbulence induce by a planar energy source (e.g. a vertically oscillating grid) the mean position of the interface can be predicted by the relation

$$H(t) = \sqrt{Kt}. \tag{1.3.3}$$

Long (1972) theorized this relation for planar forced flows in semi-infinite spaces, anyway experimental measurements in water filled tank, accord well with theory for what concern the flow far from tank walls. The values for K have been empirically determined by regression analysis

$$ln(H) = n \cdot ln(t) + \frac{1}{2} ln(K), \tag{1.3.4}$$

the theoretical value for n is obviously 0.5, though some time slightly different values have been reported (liberzon et al. 2009, Holzner eal. 2006). The value of K depends on the fluid and, at least for water, seems to increase when certain polymers are diluted in the fluid (Liberzon et al. 2009). Polymers seems to interfere with the classical mechanism of energy cascade and their effect on propagation of turbulence suggests that small scales interactions cannot be easily neglected in entrainment models.
In the early works of Corrsin (1943) and Corrsin and Kistler (1955) has been postulated

that the entrainment velocity u_a depends on the kinematic fluid viscosity ν and on the dissipation $\epsilon = 2\nu s_{ij} s_{ij}$ in the local turbulent side of the interface. Thus the entrainment velocity must scale with the dissipative characteristic velocity , i.e. the Kolmogorov velocity u_η. This is apparently in opposition with the fact that the flux of entrained fluid is determined by big scale parameters of the flow; in Holzner et al. (2009) is proposed a theory which can conciliate the small scale entrainment mechanism with the big scale rate of entrainment. They argue that the global entrainment flux, i.e. $Q = v_e A_0$, occurs through a large scale (or projected) interface area A_0, and the strongly convoluted total interface area A_η adjust itself to account for the same flux with a much smaller characteristic velocity so that

$$Q = v_e A_0 = u_a A_\eta \propto u_\eta A_\eta, \tag{1.3.5}$$

although they have not been able to find how the total area should adjust itself in such way. This hypothesis relates then the big scales with the small ones through the entrainment flux, according to this the ratio between the two areas is

$$\frac{A_\eta}{A_0} \sim \frac{v_e}{u_\eta} \tag{1.3.6}$$

being $u_\eta \sim \nu/\eta$, we have

$$\frac{A_\eta}{A_0} \sim \frac{v_e \eta}{\nu}. \tag{1.3.7}$$

Sreenivasan in his study on fractal dimensions of turbulence (Sreenivasan et al. 1989) found that

$$\frac{A_\eta}{A_0} \sim \left(\frac{\eta}{L}\right)^{2-d} \tag{1.3.8}$$

where the value found for d is $7/3$. We can now write the propagation velocity v_e as

$$v_e \sim \nu \left(\frac{L}{\eta^4}\right)^{\frac{1}{3}} = \frac{\nu}{\eta}\left(\frac{L}{\eta}\right)^{\frac{1}{3}} \tag{1.3.9}$$

which show how the propagation velocity scales with the ratio between the greatest scale in the field and the dissipative length.
Assuming that the relation $\eta/L \sim Re_L^{-3/4}$ is valid in this framework, we obtain

$$v_e \sim \frac{\nu}{\eta} Re_L^{1/4} \tag{1.3.10}$$

Must be said that at the present there is only indirect evidence for the assumption that $u_a \sim u_\eta$, no precise measurements of the local velocity of the interface are available at the present day. Since now the experiments performed in order to measure the behavior of the interface relied on PIV measurement which can extract only one vorticity component of the field with significant errors in the non-turbulent side of the interface (see for an assessment of the measurement error Westerweel et al. 2009). Holzner et al. (2009) addressed the problem with a numerical experiment of grid turbulence, they observed that the iso-surface of enstrophy (constant ω^2) evolve according to

$$\frac{\partial \omega^2}{\partial t} + u_j \frac{\partial \omega^2}{\partial x_j} = -u_a |\nabla \omega^2|. \tag{1.3.11}$$

The enstrophy balance equation on the other hand gives

$$\frac{1}{2}\frac{\partial \omega^2}{\partial t} + \frac{1}{2} u_j \frac{\partial \omega^2}{\partial x_j} = \omega_i \omega_j s_{ij} + \nu \omega_i \nabla^2 \omega_i, \tag{1.3.12}$$

from equation 1.3.11 and 2.3.22 we can obtain an equation for u_a composed by an inviscid and a viscous contribution

$$u_a = -\frac{\omega_i \omega_j s_{ij}}{|\nabla \omega^2|} - \frac{\nu \omega_i \nabla^2 \omega_i}{|\nabla \omega^2|}. \tag{1.3.13}$$

In their simulation Holzner et al. found a u_a about two time smaller than u_η, moreover they found that locally the viscous term strongly prevails over the inviscid interaction strain-enstrophy.

A note must be done about the range of validity of the aforementioned theories, all the data and the studies available at the present day involve modest Reynolds numbers, the usual Re goes from 10^3 for wakes and jets (e.g. Westerweel et al., Mathew et al., Khashehchi et al.) experiments to few decades for some grid induced turbulence (Holzner et al. , Liberzon et al.). At the much higher Reynolds number usually encountered in applicative fields, the behavior of the interface has not been yet extensively studied, due to the limitations of both measurement instruments and computational simulations.

Chapter 2

Diffusion of decaying turbulence

2.1 Entrainment in decaying turbulence

The simplest model of a turbulent flow is the case of homogeneous isotropic turbulence.Such flow does not find any equivalence in a real experiment, though some flows like grid generated turbulence tend to the homogeneous isotropic behavior; yet it is an useful starting point for the comprehension of turbulence mechanics since it possesses certain characteristics shared by all commonly studied turbulent flows. Homogeneity of the flow means statistical invariance of flow quantities with respect to translation in any direction, whereas the isotropy assumption brings statistical invariance with respect to rotations and reflections of the coordinate system.
In this investigation we started then creating a field of homogeneous isotropic turbulence, from such field we generated the initial conditions for the interface simulation then we simulated the diffusion of the decaying turbulence in such domain. The present work of thesis belongs to a more general research project aiming at studying the turbulent/non-turbulent interface. Here we start with the analysis of the turbulent/non-turbulent interface with decaying turbulence. The results obtained will be used then as starting point for the study of turbulent/non-turbulent interface with forced turbulence. The parameters of the simulation are hence intended to match the parameters of previous experiments with shearless interfaces in water filled tank (Holzner et al. 2006, Liberzon et al. 2009). The simulation of unforced, freely evolving turbulence differs in many aspect from such experiments, nevertheless has shown to share many aspect in interface behavior with them.

2.2 Numerical simulation

For both the generation of the initial turbulent field and the simulation of the decaying turbulent flow, a pseudo-spectral DNS code has been used. Pseudo-spectral codes solve the partial differential equation system generated by Navier-Stokes equations in the Fourier space. To keep the code efficient non-linear terms are transformed back to the physical space and there estimated; this operation has a computational cost of the order of $\mathcal{O}(N\,log\,N)$ (thanks to fast Fourier transform algorithms) while the estimation via convolution of the non linear terms in the Fourier space require $\mathcal{O}(N^2)$operations, thus the choice for the former.It is to note that Pseudo-spectral codes have the important feature of the spectral accuracy property. The code utilized in the present work has already been used in previous works on homogeneous isotropic turbulence (De Angelis et al. 2005).

2.2.1 Set of initial conditions

As starting point a cubic domain of homogeneous isotropic turbulence had been created. All the initial conditions for the interface simulations in the present work have been originated from a unique run of a $128 \times 128 \times 128$ grid points domain.
The equation of fluid motion in the Fourier space used in the present work is

$$\frac{\partial \hat{\mathbf{u}}}{\partial t} = \hat{\mathbf{H}} - \nu k^2 \hat{\mathbf{u}} + \hat{\mathbf{F}}, \tag{2.2.1}$$

where $\hat{\mathbf{H}}$ and $\hat{\mathbf{F}}$ are terms respectively associated to the non linear and the forcing term through

$$\hat{\mathbf{H}} = \hat{\mathbf{h}} - \frac{\mathbf{k}}{k^2}(\hat{\mathbf{k}} \cdot \hat{\mathbf{h}}) \tag{2.2.2}$$

$$\hat{\mathbf{F}} = \hat{\mathbf{f}} - \frac{\mathbf{k}}{k^2}(\hat{\mathbf{k}} \cdot \hat{\mathbf{f}}). \tag{2.2.3}$$

The terms $\hat{\mathbf{f}}$ and $\hat{\mathbf{h}}$ are respectively the Fourier coefficient of forcing term and of the non linear term

$$h_i = -u_j \frac{\partial u_i}{\partial x_j}. \tag{2.2.4}$$

The forcing term has the goal to force on a limited band-width around a given wave number k^2

$$k^2 = \sqrt{k_x^2 + k_y^2 + k_z^2} \tag{2.2.5}$$

$$k_{min}^2 \leq k^2 \leq k_{max}^2, \tag{2.2.6}$$

with a random amplitude which follow a Gaussian distribution over the assigned wave numbers range.

$$\hat{f}_i(k_x, k_y, k_z, t) = \hat{f}_0 \cdot \frac{e^{-\frac{1}{2}(\frac{\sqrt{k^2-\mu^2}}{\sigma})^2}}{\sigma} \tag{2.2.7}$$

The range chosen is $3.2 \leq k^2 \leq 6.8$ around the wave numbers with $\mu^2 = 5$ and $\sigma = 6$.
The total temporal length of the simulation has been of about 72 integral time scales t_0.

$$t_0 = \frac{L_0}{u_{rms}} \tag{2.2.8}$$

After the statistical stationarity has been reached, 25 independent initial fields have been selected.
The Reynolds number has been computed as

$$Re_\lambda = \frac{u_{rms} \cdot \lambda}{\nu}, \tag{2.2.9}$$

and the Taylor microscale λ has been computed as

$$\lambda = \sqrt{\frac{5 \cdot u_{rms}}{\langle \omega^2 \rangle}} \tag{2.2.10}$$

n^{er} *of fields*	$N_x \times N_y \times N_z$	L_x,L_y,L_z	Re	Re_λ	λ	η	Δt	t_0
25	$128 \times 128 \times 128$	2π	120	52	0.242	0.017	0.001	0.23

Table 2.1: Initial fields parameters

In order to simulate the interface, a field composed by two neighboring identical velocity fields of $128 \times 128 \times 128$ points has been created; due to the periodic boundary conditions, the interface between the two fields this does not generate discontinuities of any

sort. The new initial velocity field $\mathbf{u_o}(x, y, z)$ is then multiplied by a junction function which smoothly brings to zero the velocity field in half domain (as proposed by Tordella et al. 2008); the junction function is constructed in such a way to retain the periodicity of the field on the boundaries. The junction function is

$$\mathbf{u}(x, y, z) = \mathbf{u_o}(x, y, z) \cdot p(x) \tag{2.2.11}$$

$$p(x) = \frac{1}{2}\left[1 + tanh\left(a \cdot \frac{x}{L}\right) \cdot tanh\left(a \cdot \frac{x - L/2}{L}\right) tanh\left(a \cdot \frac{x - L}{L}\right)\right] \tag{2.2.12}$$

Here the constant a is a parameter which affects the initial width of the interface and L is the domain length. For the current simulations the parameter a has been set at 6π, the values have been chosen in order to grant an initial thickness large enough to be resolved.

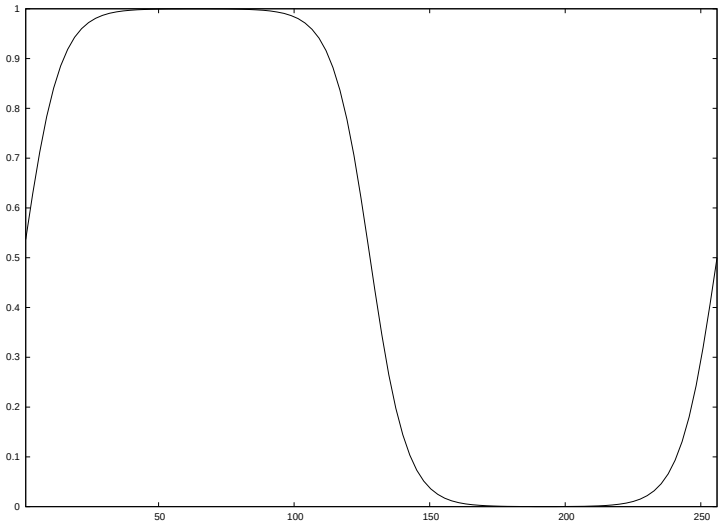

Figure 2.2.1: The smoothing function $p(x)$ for the initial interface

The fields generated is such way have been then let freely evolve for 2000 time steps Δt (or 10 integral time scales), the turbulence in them spreading and decaying. The result is a series of velocity field constituted by a center core of approximatively homogeneous isotropic turbulence, while the field become more and more anisotropic closer to the interface. As can be seen in the figure each field consist of two interfaces thus a total of 50 interfaces over 20 time intervals each constitute the data-set we have used for our study.

The spatial resolution , i.e. the smallest structure that can be resolved is given by smallest wave number of the field, namely

$$k_{min} = \frac{2\pi}{128} = 0.049. \tag{2.2.13}$$

2.3 Results

From each of the 25 initial condition we have started an independent integration without forcing. From each of those 20 fields have been saved at regular time intervals, for a total of 500 fields and 1000 interfaces. Anyway only about half of these have been taken in account for the following results, precisely only all the temporal step greater then it=1200 constitute the data set for the analysis. Such reduction has been necessary in order to exclude transitory phenomena and let the flow to lose every memory of the artificious initial interface. Almost all results in the present work are spatially averaged in planes normal to the direction of diffusion, i.e. the coordinate x. These statistic in each plan have been then ensemble averaged with its symmetric counterpart respect the centerline of the turbulent part of the flow; finally the results have been ensemble averaged over all the 25 fields. Thus the statistics that will be presented in this chapter come from the evaluation of 819.000 points for each plane $y - z$ and each time interval, number which has shown large enough for the convergence of the statistics.

2.3.1 Flow characteristics

The flow obtained from our simulation is constituted by a core of almost homogeneous isotropic turbulence which spreads and decay in an irrotational fluid. Due to the imposition of periodic condition, at every boundary the flow is imposed to be the same on opposite sides of the domain box, hence the two apparently separate interfaces actually propagate from the same turbulent core. The diffusion of turbulence from this core is continuously counteracted by the dissipation in such a way that the turbulence cannot fill the field, and the two interfaces never come in contact in the temporal range of the simulation. For the purpose of the present work two sections of the turbulent flow are of particular interest: the center plane of the turbulent flow and the average position of the initial interface (x=0), which will be indicated hereafter simply as turbulent core and interface, respectively. The

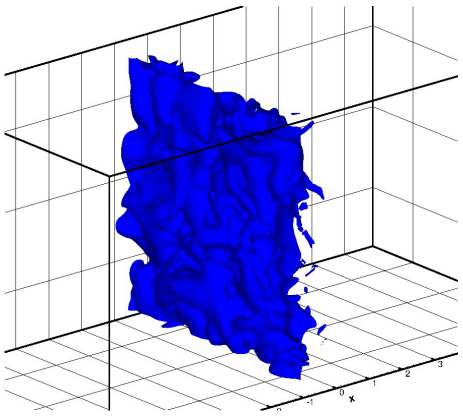

Figure 2.3.1: Iso-surfaces of kinetic energy: 10% threshold.

former is useful to show the differences in decay rates and other flow properties respect the ideal case of homogeneous isotropic turbulence; the latter instead is indicative of the flow evolution in the volume of flow affected by the interface.
The interface region nevertheless change sensibly in its shape with time, ever producing new turbulent structures, bubbles of vorticity and engulfing pockets of laminar flow.
As can be seen from the probability density functions of the longitudinal velocity fluctuations (figures 2.3.2 2.3.3), the field is strongly intermittent in proximity of the interface and negatively skewed; on the other hand field in the turbulent core shows an almost symmetrical distribution and a more regular profile.
The anisotropy levels, defined as

$$\frac{\langle u_i^2 \rangle}{\langle u^2 \rangle + \langle v^2 \rangle + \langle w^2 \rangle}, \tag{2.3.1}$$

indicates that the relative weight of velocity fluctuations in the longitudinal direction slowly grows in the turbulent interface, in correspondence of which it start to peaks fast. The evaluation of the anisotropy is truncated at the beginning of the laminar side where the ratio is biased by the numerical noise.

2.3.2 Energy decay

The average kinetic energy of the field results to be a function of both time and x coordinate. The profiles shown in figure 2.3.5 evidence such dependence: at a given time, the

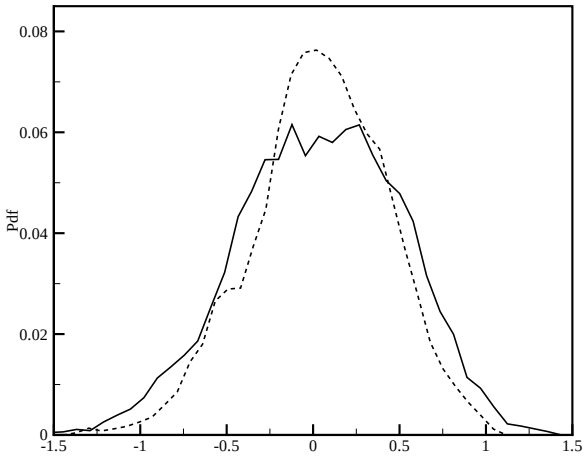

Figure 2.3.2: Pdf of u in a plane centered in the turbulent core. Solid line: t=1.8, dashed line t=2.0

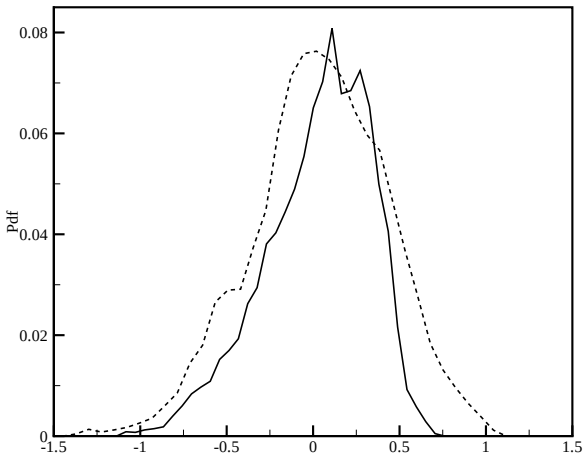

Figure 2.3.3: Pdf of u at different positions. Dashed line: turbulent core, solid line: interface plane (x=0).

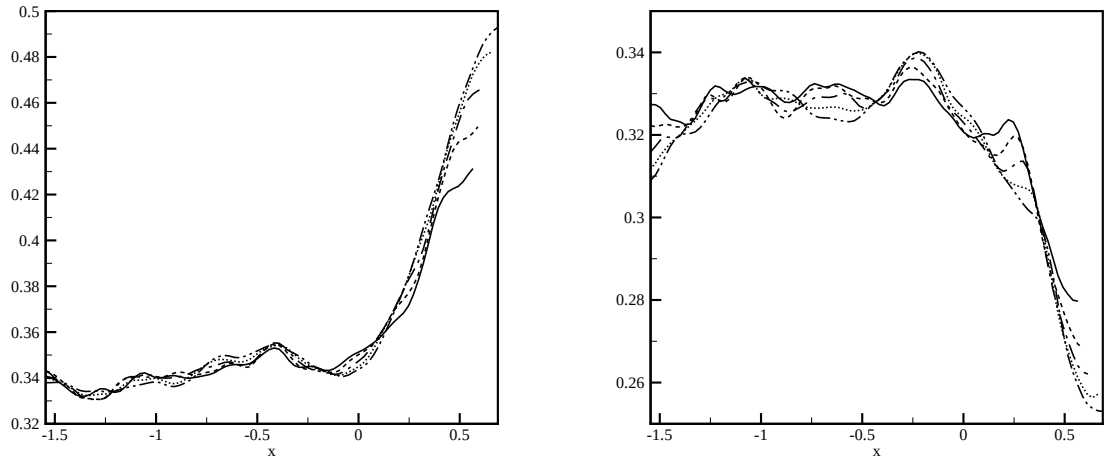

Figure 2.3.4: Spatial variation of the anisotropy $\frac{\langle u^2 \rangle}{\langle u^2+v^2+w^2 \rangle}$ (left) and $\frac{\langle v^2 \rangle}{\langle u^2+v^2+w^2 \rangle}$ (right) . t/t_0 from 5.2 (solid line) to 8.6 (dash-dotted).

kinetic energy keeps a flat profile until the interface is approached then it rapidly drops to zero in few Taylor microscales. The figure also shows the evolution with time of turbulent kinetic the energy: in the turbulent core of the flow it decays as expected, while a slightly increase in the velocity fluctuations can be observed in the initially non-turbulent region.
The introduction of the interface brings an increase of effective dissipation with respect the case of homogeneous isotropic turbulence. In the turbulent core of the flow, where the turbulence is in first approximation still homogeneous and isotropic, the decay rate is increased due to the energy flux toward the interface. The inhomogeneity introduced by the presence of the interface produce spatial energy fluxes which tend to homogenize the flow. Hence the turbulent core release energy through such energy fluxes and experience an increased effective dissipation.
In figure 2.3.6 the normalized kinetic energy of the turbulence core and of the homogeneous isotropic turbulence are compared. Both, after an initial evolution, follow approximatively a classical power law and the homogeneous isotropic has the decay of predicted by Kolmogorov theory of t^{-1}. The turbulent flow with the interface shows instead a larger decay rate of $t^{-\frac{7}{5}}$, which is mainly due to the energy flux toward the interface. Hence the interface act as a sink of energy for the turbulent core.
It can be seen that the time variation in kinetic energy, i.e. dissipation, is a function of

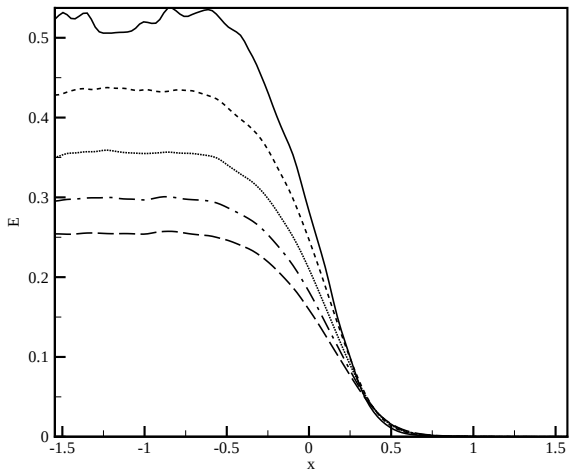

Figure 2.3.5: Temporal evolution of the average kinetic energy in the y-z plan, solid line: t/t_0 =5.2 , dashed: 6.0 , dotted: 6.9 , dash-dot: 7.8 , long dash: 8.6 (long dashed)

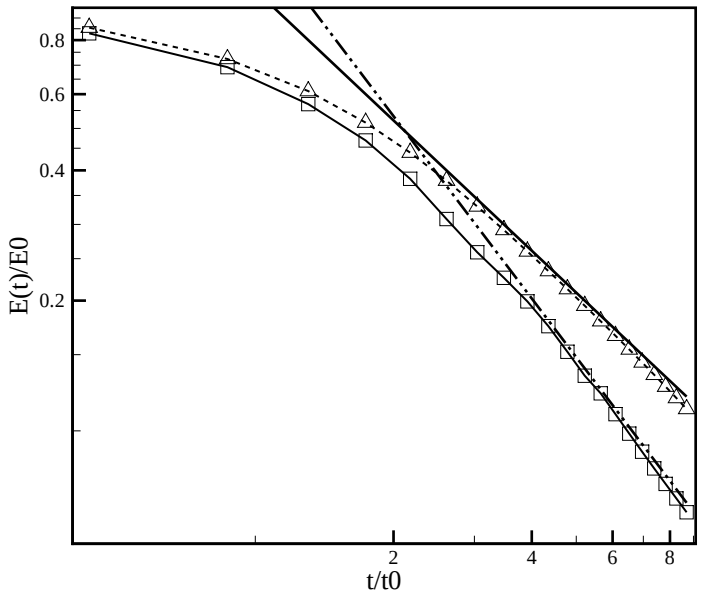

Figure 2.3.6: Normalized kinetic energy decay of a box of homogeneous isotropic turbulence (triangles) and the turbulent core of the flow with the interface (squares). Solid bold: t^{-1}. Dash-dot: $t^{-\frac{7}{5}}$.

the longitudinal position x. In figure 2.3.7 such dependence is shown in logarithmic scale; the slope of the decay of kinetic energy become less and less steep increasing the distance from the turbulent side of the flow, until eventually a zone of energy growth is reached.

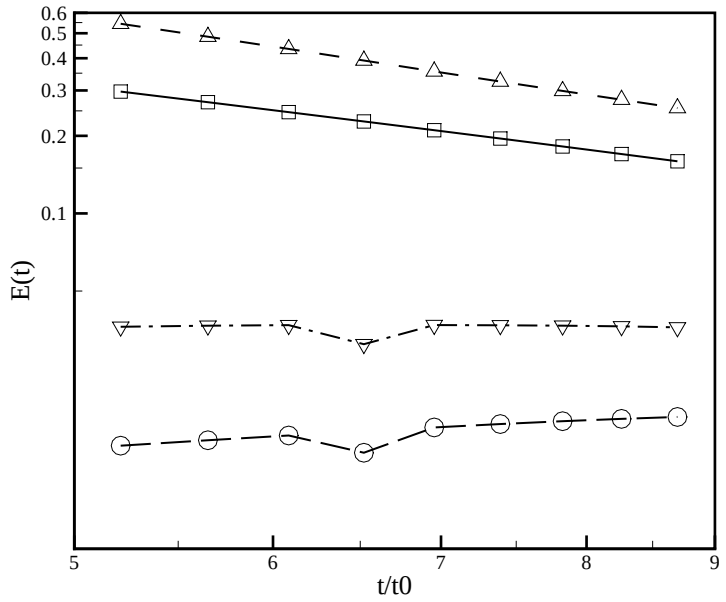

Figure 2.3.7: Time variation of kinetic energy in different planes: turbulent core (triangles), interface x=0 (squares), x=0.39 (triangles), x=0.5 (circles)

As expected the local Taylor microscale depends on the distance from the turbulent side and tend to grow with x. Even if not theoretically rigorous at such low Reynolds numbers, we adopted the classical relation between dissipation and Taylor microscale in order to estimate λ

$$\epsilon = 15\nu \frac{\langle u_i^2 \rangle}{\lambda}. \tag{2.3.2}$$

The dissipation on the other hand is

$$\epsilon = 2\nu \left\langle s_{ij} s_{ij} \right\rangle, \tag{2.3.3}$$

which in isotropic turbulence is equivalent to the term $\langle \omega_i^2 \rangle$ and as will be seen in the following chapters, a good correspondence persist even when the isotropy hypothesis is

lost (at least for what concern the order of magnitude and behavior required for scales considerations, see figure 2.3.5). The Taylor microscale then grows both in time and with the position, following the decrease in energy content of the flow (figures 2.3.8and2.3.9), hence the Re_λ evolves accordingly. In the studied temporal range, the turbulent side λ vary from 0.26 to 0.33, while Re_λ decays from 37 to 28.

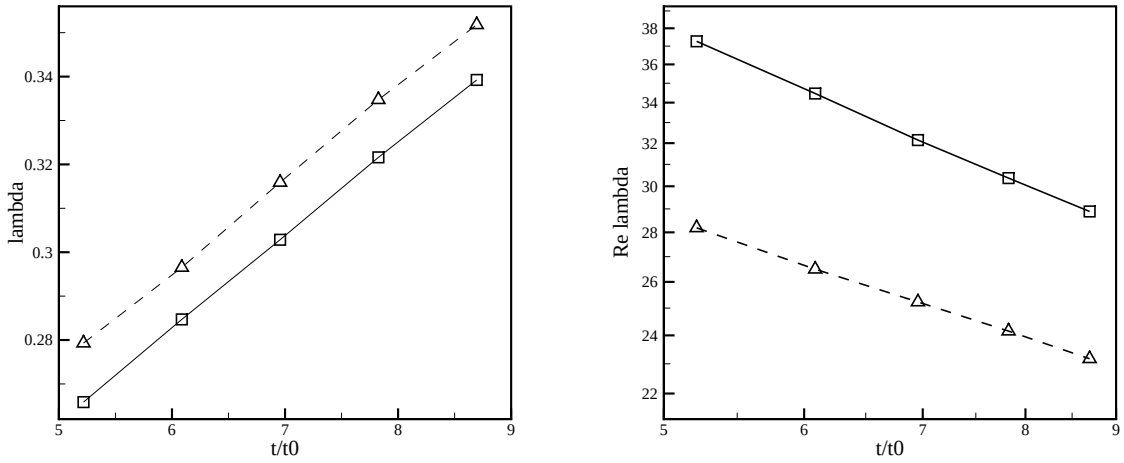

Figure 2.3.8: Evolution of the Taylor microscale λ (left) and Re_λ (right). Solid line: turbulent core, dashed: interface ($x = 0$)

Evidently the Kolmogorv scale $\eta = (v^3/\epsilon)^{1/4}$, grows spatially moving toward the irrotational flow following the decrease in energy content of the flow (figure 2.3.9), though the evolution of the Kolmogorov scale has a much smoother profile. To note that η highlights a steep decay of the small scales in the interface region.

2.3.3 Enstrophy and energy scales

As introduced in the first chapter, one of the essential quantitative markers of turbulence is vorticity. The square of the vorticity divided by two is called enstrophy and is a quantity useful for characterizing a variety of turbulent phenomena. Moreover enstrophy thresholds has been often used as detection mechanism for the turbulent/non-turbulent interface (see Holzner et al. 2006, 2007), since a sharp jump in enstrophy levels can be observed crossing the interface.

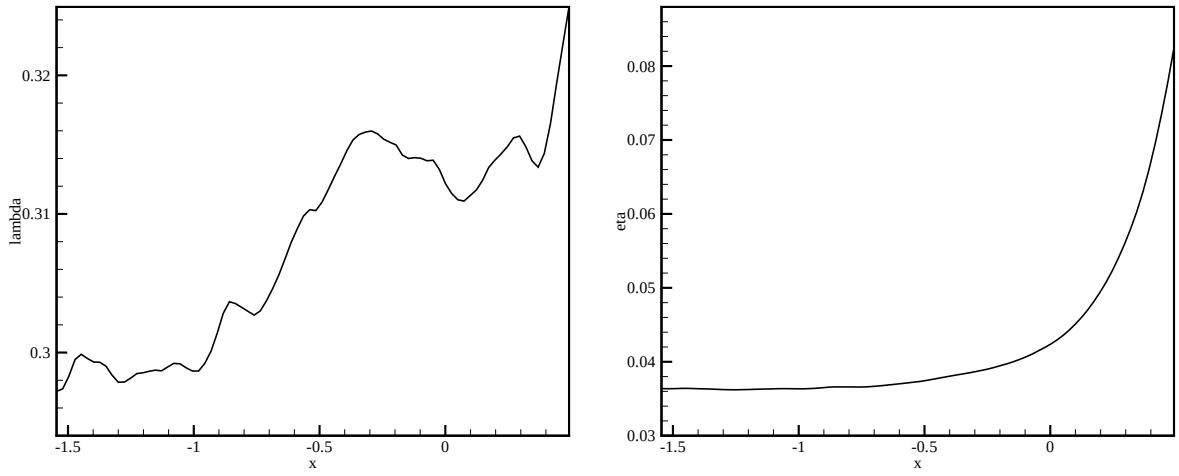

Figure 2.3.9: Spatial variation of the Taylor microscale λ (left) and Kolmogorov sale η (right). t/t_0 =6.9

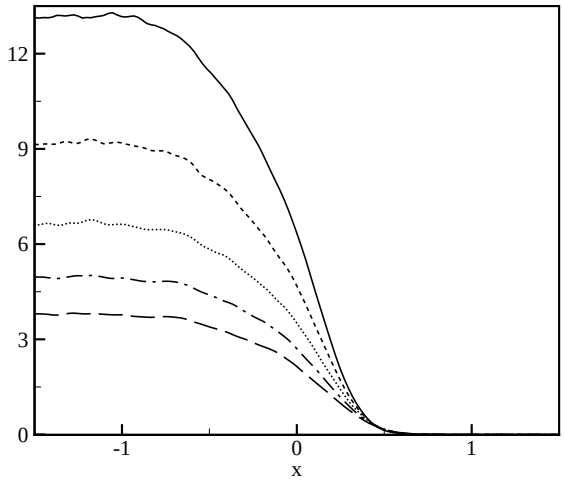

Figure 2.3.10: Temporal evolution of enstrophy $\left\langle \frac{\omega_i^2}{2} \right\rangle$,solid line: t/t_0 =5.2 , dashed 6.0, dotted: 6.9 , dash-dot: 7.8 , long dash: 8.6 (long dashed)

Figure 2.3.10 shows the averaged profiles of enstrophy across the interface. The graph show as enstrophy decrease to a zero level in the non-turbulent side, while it has a quasi-constant value in the turbulent side of the field. The enstrophy follows the same profiles observed in previous experiments with grid induced turbulence (Holzner et al. 2007) and DNS of wakes (Bisset et al. 2001).

The simulation of the Navier-Stokes equation in the Fourier space give an easy way to compute both energy and enstrophy spectra of the field. In fact if the Fourier coefficient $\hat{u}_i(k_x, k_y, k_z)$ and $\hat{\omega}(k_x, k_y, k_z)$ are known, the spectrum can be obtained by multiplying each term for its complex conjugate. In the present study the spectra has been evaluated in each section y-z of the field, to evaluate the distribution of energy and enstrophy in both the longitudinal direction and plane wave numbers $k_y - k_z$, thus obtaining the functions $E_k(x, k_y, k_z)$ and $\Omega_k(x, k_y, k_{z)}$. Since the flow is isotropic in the y-z planes, we will consider the integral of the spectral energy and enstrophy over a circular shell in the $k_y - k_z$ space, i.e $E_k(x, k)$ and $\Omega_k(x, k)$.

The plot of E_k (figure 2.3.11) highlights three different behaviors. The first one is that across the interface persists an intermediate range of scales which retains energy levels comparable with the ones found into the turbulent core. The second and the third one is a larger and smaller decrease of energy at small and large scale respectively, crossing the interface. This behavior may be induced by the combination of two effects. The first one could be the erosion of small scales due to dissipation which persists crossing the interface as will be shown in the spectral enstrophy after. The second could be the orientation of the spatial energy fluxes from the turbulent core towards large scale motion. It is interesting to note that the protrusion of large scale fluctuations, which have a much lower spatial decay with respect all the other scales, is characterized essentially by irrotational motion as will shown below whit spectral enstrophy.

The spectral enstrophy Ω_k (figure 2.3.12) have a much flatter spatial decay confronted to the kinetic energy spectra, i.e. all the scales exhibit nearly the same decay along x. The comparison between the kinetic energy spectrum and the enstrophy spectrum indicate a higher dissipation of kinetic energy at small scales, which correspond to a slow spatial decay of enstrophy levels in such region. The decay of large scale of enstrophy with x indicates that the large scale protrusions seen in the energy spectra are probably due to irrotational velocity fluctuations in the laminar flow.

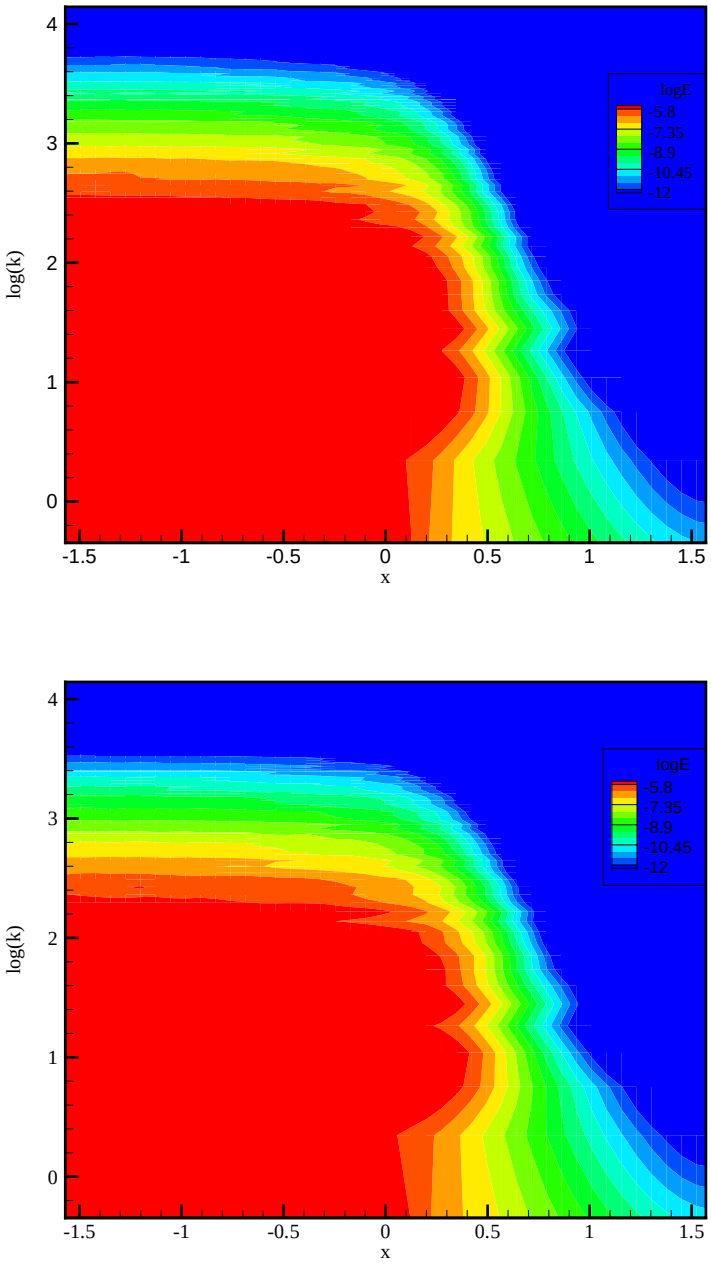

Figure 2.3.11: Contour plot of $E_k(x,k)$. t/t$_0$ =5.2. Low t/t$_0$ =6.9.

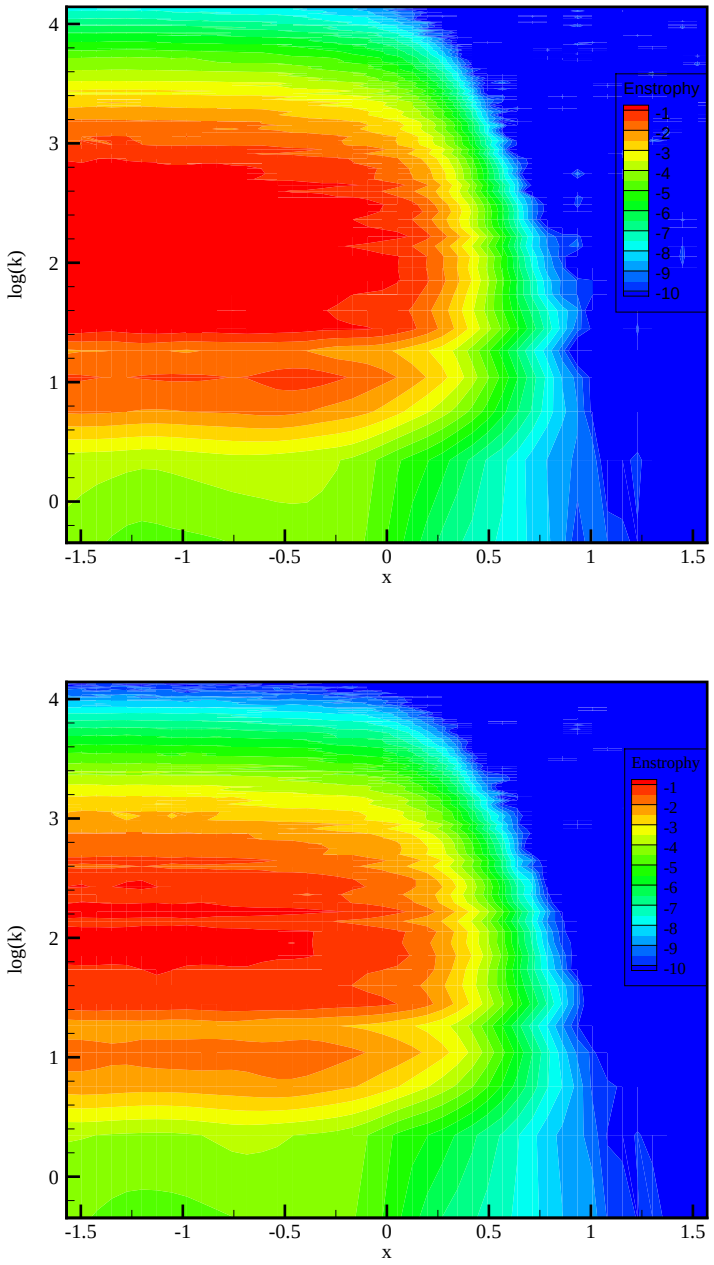

Figure 2.3.12: Contour plot of the $\Omega_k(x,k)$. high: t/t_0 =5.2. Low t/t_0 =6.9.

2.3.4 Enstrophy balance equation

Entrainment is a process where turbulence generates other turbulence in an irrotational region, hence the study of the local production or dissipation of vorticity helps to understand the mechanics of the underlying entrainment process. The equation for the local balance of enstrophy is

$$\frac{1}{2}\frac{D}{Dt}\left\langle \omega_i^2 \right\rangle = \left\langle \omega_i \omega_j s_{ij} \right\rangle + \nu \left\langle \omega_i \nabla^2 \omega_i \right\rangle \tag{2.3.4}$$

where the term s_{ij} is the strain rate and is given by

$$s_{ij} = \frac{1}{2}\left(\frac{\partial u_i}{\partial x_j} + \frac{\partial u_j}{\partial x_i}\right). \tag{2.3.5}$$

The first right-hand side term of the 2.3.4 is the turbulent stretching of fluctuating vorticity while the second term on the right is the viscous dissipation; re-expressing the total derivative, equation 2.3.4 becomes

$$\frac{1}{2}\frac{\partial}{\partial t}\left\langle \omega_i^2 \right\rangle + \frac{1}{2}\left\langle u_j \frac{\partial}{\partial x_j}(\omega_i^2) \right\rangle = \left\langle \omega_i \omega_j s_{ij} \right\rangle + \nu \left\langle \omega_i \nabla^2 \omega_i \right\rangle. \tag{2.3.6}$$

The second term on the left side can be also written as

$$\left\langle u_j \frac{\partial}{\partial x_j}(\omega_i^2) \right\rangle = -\frac{\partial}{\partial x_j}\left\langle \omega_i^2 u_j \right\rangle + \left\langle \omega_i^2 \frac{\partial u_j}{\partial x_j} \right\rangle, \tag{2.3.7}$$

we have hence that the left side of the equation can be written as

$$\frac{1}{2}\frac{\partial}{\partial t}\left\langle \omega_i^2 \right\rangle + \frac{1}{2}\left\langle u_j \frac{\partial}{\partial x_j}(\omega_i^2) \right\rangle = \frac{1}{2}\frac{\partial}{\partial t}\left\langle \omega_i^2 \right\rangle + \frac{1}{2}\left\langle \frac{\partial}{\partial x_j}(\omega_i^2 u_j) \right\rangle - \frac{1}{2}\left\langle \omega_i^2 \frac{\partial u_j}{\partial x_j} \right\rangle. \tag{2.3.8}$$

The last term is zero due to the zero-divergence of the velocity field, thus we have that the enstrophy evolution is

$$\frac{1}{2}\frac{\partial}{\partial t}\left\langle \omega_i^2 \right\rangle = -\frac{1}{2}\left\langle \frac{\partial}{\partial x_j}(\omega_i^2 u_j) \right\rangle + \left\langle \omega_i \omega_j s_{ij} \right\rangle + \nu \left\langle \omega_i \nabla^2 \omega_i \right\rangle. \tag{2.3.9}$$

For the the second term on the right side we have

$$\left\langle \omega_i \frac{\partial^2 \omega_i}{\partial x_j^2} \right\rangle = -\frac{\partial^2}{\partial x_j^2} \left\langle \omega_j^2 \right\rangle + 2 \left\langle \frac{\partial \omega_i}{\partial x_j} \frac{\partial \omega_i}{\partial x_j} \right\rangle, \tag{2.3.10}$$

the consequence is that

$$\nu \left\langle \omega_i \nabla^2 \omega_i \right\rangle = \frac{\nu}{2} \frac{\partial^2}{\partial x_j^2} \left\langle \omega_j^2 \right\rangle - \nu \left\langle \frac{\partial \omega_i}{\partial x_j} \frac{\partial \omega_i}{\partial x_j} \right\rangle, \tag{2.3.11}$$

thus the final relation for the enstrophy balance equation is

$$\frac{1}{2} \frac{\partial}{\partial t} \left\langle \omega_i^2 \right\rangle = -\frac{1}{2} \frac{\partial}{\partial x_j} \left\langle \omega_i^2 u_j \right\rangle + \left\langle \omega_i \omega_j s_{ij} \right\rangle + \frac{\nu}{2} \frac{\partial^2}{\partial x_j^2} \left\langle \omega_i^2 \right\rangle - \nu \left\langle \frac{\partial \omega_i}{\partial x_j} \frac{\partial \omega_i}{\partial x_j} \right\rangle. \tag{2.3.12}$$

This last relation evidence how the evolution of enstrophy is the result of four contributes. The term $\nu \left\langle \frac{\partial \omega_i}{\partial x_j} \frac{\partial \omega_i}{\partial x_j} \right\rangle$ is always definite positive hence its contribute to enstrophy balance is dissipative, that is why it is usually called viscous dissipation. The term $\frac{\nu}{2} \frac{\partial^2}{\partial x_j^2} \left\langle \omega_j^2 \right\rangle$ represents the diffusion of vorticity due the viscosity. Must be noted that the decomposition in 2.3.11 is not unique, there is an infinite number of possibilities to represent $\nu \left\langle \omega_i \nabla^2 \omega_i \right\rangle$ as a sum of a dissipation and a flux term (i.e. as a divergence of some vector) (Holzner 2007). There is no way to define dissipation (i.e. to choose one among many purely negative expressions) of enstrophy as it is not an inviscidly conserved quantity, unlike the kinetic energy (Tsinober 2001). Nevertheless such decomposition retain its utility in understanding some of the underlying physical aspects of turbulent diffusion, as will be seen soon.

The term $\left\langle \omega_i \omega_j s_{ij} \right\rangle$ is responsible for enstrophy production and arises from the interactions between the vorticity and the rate of strain tensor s_{ij}. It is usually considered as a positive term, although so far no theoretical arguments in favor of positiveness of $\left\langle \omega_i \omega_j s_{ij} \right\rangle$ have been given (Tsinober 2001). Last, the term $-\frac{1}{2} \frac{\partial}{\partial x_j} \left\langle \omega_i^2 u_j \right\rangle$ is the gradient of the interactions between vorticity and velocity fluctuations, represent how vorticity is transported by velocity fluctuations and we will call it inertial diffusion. Our data are averaged in the $y - z$ planes, where homogeneity is conserved. Thus equation 2.3.12 retains only the x derivatives of the averages, leading to

$$\frac{1}{2}\frac{\partial}{\partial t}\left\langle \omega_i^2 \right\rangle = -\frac{1}{2}\frac{\partial}{\partial x}\left\langle \omega_i^2 u_j \right\rangle + \left\langle \omega_i \omega_j s_{ij} \right\rangle + \frac{\nu}{2}\frac{\partial^2}{\partial x^2}\left\langle \omega_i^2 \right\rangle - \nu \left\langle \frac{\partial \omega_i}{\partial x_j}\frac{\partial \omega_i}{\partial x_j} \right\rangle . \qquad (2.3.13)$$

In the case of decaying turbulence the global balance lead to a continuous dissipation of vorticity due to the viscosity. Nevertheless in our case, where the entrainment is undergoing, there should be zone of positive variation of vorticity $\frac{\partial}{\partial t}\left\langle \omega_i^2(x) \right\rangle > 0$. This positive variation, in a globally turbulence-decaying frame,(figure 2.3.13) can be only attributed to the entrainment of irrotational fluid in the turbulent mass and permits to identify where the entrainment rate reaches its maximum, see inset of figure 2.3.13

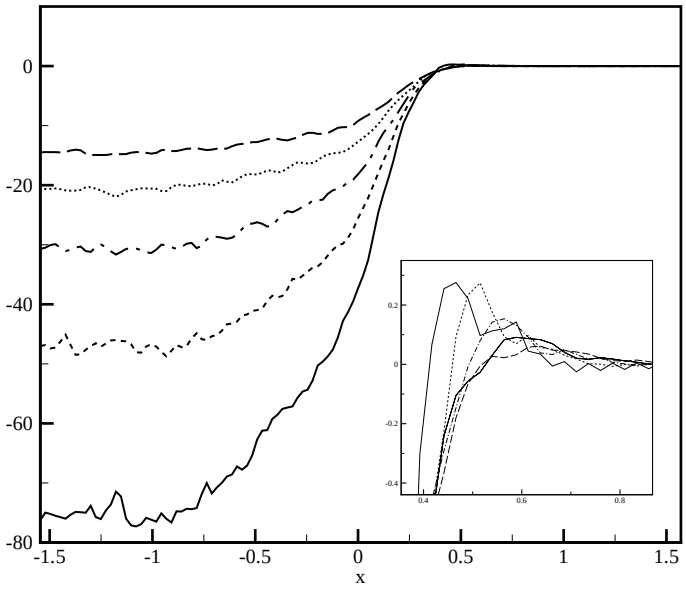

Figure 2.3.13: Plot of the term $\frac{1}{2}\frac{\partial}{\partial t}\left\langle \omega_i^2 \right\rangle$, time step from t/t_0=5.2 (lowest level) to 8.6. In the magnification the zone of positive enstrophy variation.

The position of such maxima results to be forward respect the points at 10% threshold of enstrophy shown in figure2.3.23 and forward respect the peaks of inertial and viscous diffusion that will be shown in what follows.

Figure 2.3.15 illustrate the components of enstrophy production for t=2.0. As mentioned above the production term is positive in all the field, due to the fact that turbulence is de-

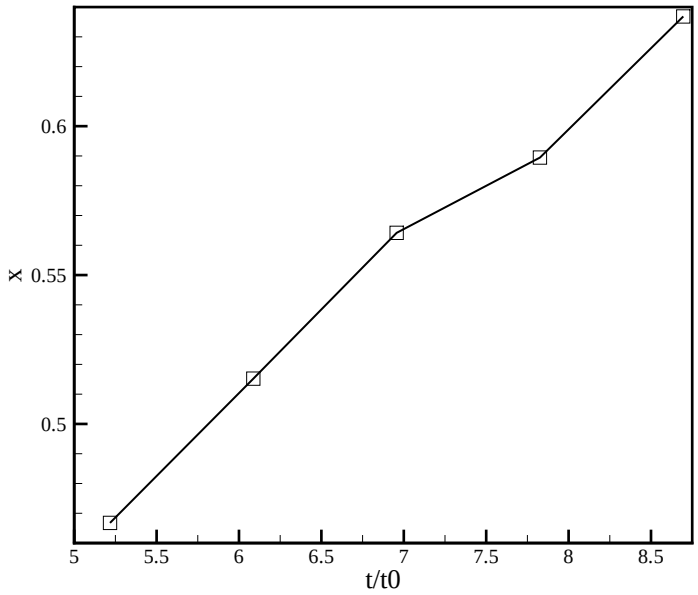

Figure 2.3.14: Position of the enstrophy balance maximum.

caying, it is about a half of the dissipation term. The latter dominate the enstrophy balance equation in the turbulent core, only in the outbounds of the interface region it reaches values comparable with the three other terms. More intersting are the terms of viscous and inertial transport since these terms are responsible for the advancement of the interface. These two terms start rising while getting closer to the interface and slowly return to zero once crossed it. The inertial term result always sensibly greater then the viscous term and , around the interface, it result greater then the production term. This suggest that in such region, the transport by velocity of vorticity prevails over the amplifying interactions between vorticity field and strains.

The net fluxes of both the inertial and viscous diffusion have been analyzed in order to better understand the contribution in turbulent entrainment. The results are illustrated in figure 2.3.16 where the dominance of the inertial flux over viscous flux is evident. The inertial flux thus draws vorticity from the turbulent core and transports it toward the interface, before which it reaches its maximum. The viscous flux remains at least one order of magnitude less than the inertial flux and reach its maximum intensity slightly closer to the laminar field. Hence from this picture it appears that inertial fluctuations plays a central

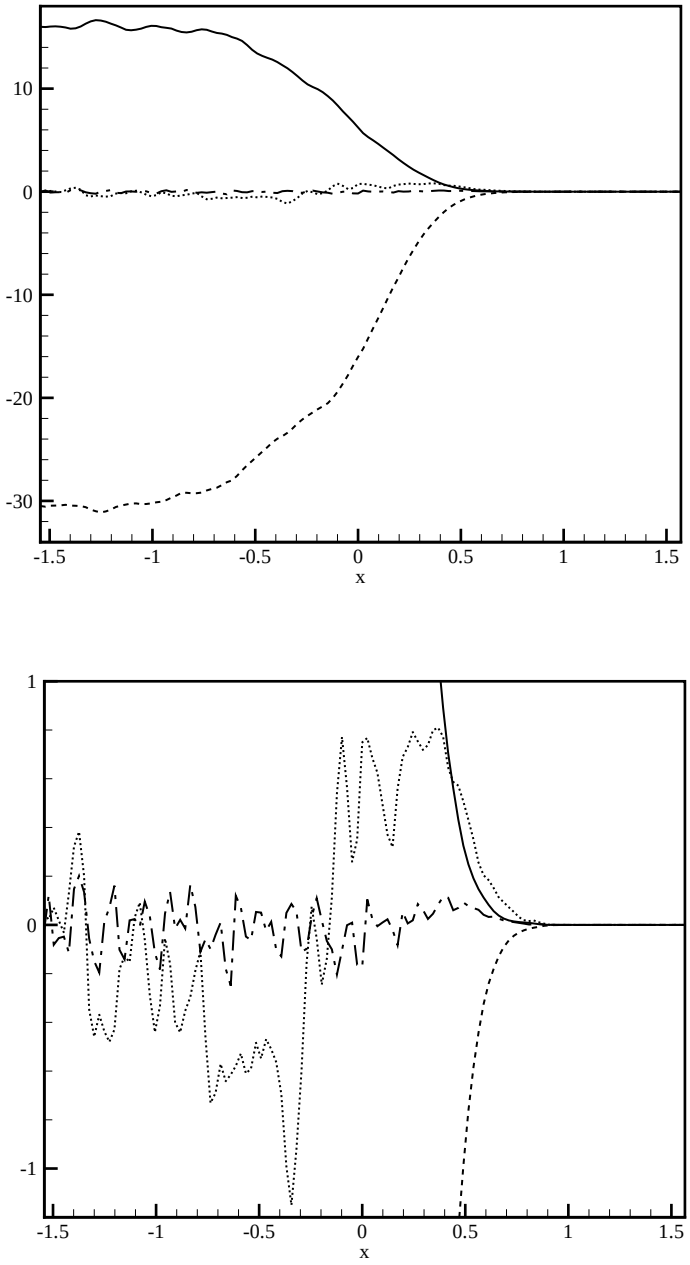

Figure 2.3.15: Enstrophy balance terms. Solid line: production $\langle \omega_i \omega_j s_{ij} \rangle$, dashed line: dissipation term $-\nu \left\langle \frac{\partial \omega_i}{\partial x_j} \frac{\partial \omega_i}{\partial x_j} \right\rangle$, dotted line: inertial diffusion$-\frac{1}{2} \frac{\partial}{\partial x} \langle \omega_i^2 u \rangle$, dashed and dotted line: viscous diffusion $\frac{\nu}{2} \frac{\partial^2}{\partial x^2} \langle \omega_i^2 \rangle$. (below) Magnification of the inertial and viscous diffusion. t/t_0= 8.6

role in transporting rotational flow from the high turbulence levels of the core toward the interface. Whereas, at the interface the intensity of the fluctuations is small and the propagation of rotational fluid toward the laminar region become a mechanism dominated by molecular viscosity.

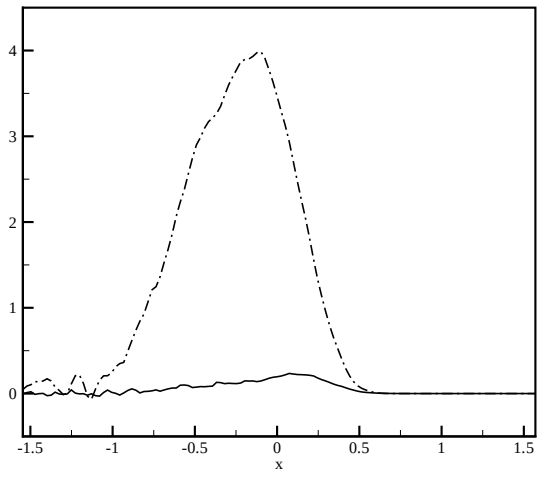

Figure 2.3.16: Viscous flux $\frac{\nu}{2}\frac{\partial}{\partial x}\langle\omega_i^2\rangle$ (solid line) and inertial flux $-\frac{1}{2}\langle\omega_i^2 u\rangle$ (dash-dotted line). t/t_0=8.6

The temporal variation of inertial flux (figure 2.3.17, left) does not evidence a significant movement of its peaks, confirming that the dependence of this process on the inertial mechanisms of the the turbulent core, which position remain unaltered in time. The analysis of the components of the inertial flux (figure 2.3.17, right) shows as expected stronger contribution of the terms of transversal vorticity. These are responsible in generating the convoluted protrusion of vorticity which can be seen in the interface visualizations. Previous authors reported the inertial flux to be globally zero at the interface for entrainment in jets (Westerweel et al. 2009). The inertial component $v \cdot \omega_z^2$ has been obtained by the PIV measure of the planar vorticity and velocity fields. The *pdf* of such component evidenced a strongly intermittent but symmetrical profile. The authors hypothesized than that at the interface, the contribution two of counterotating adjacent vortexes would lead to a zero inertial flux (as seen in figure 2.3.18).
In our simulation a relevant flux of inertial transport has been found and also the *pdf* of the inertial term seems to confirm it. The longitudinal term $-\frac{1}{2}\langle\omega_x^2 u\rangle$ and the transverse term

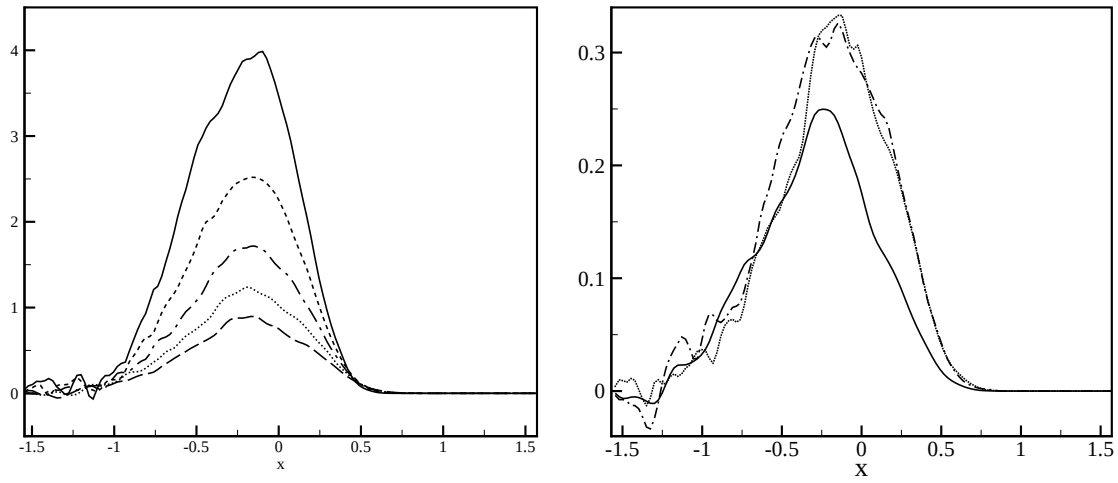

Figure 2.3.17: (Right) Temporal evolution of the inertial flux, from t/t_0= 1.2 (highest level) to 8.6. (Left) Components of the inertial flux: Solid line:$-\frac{1}{2}\left\langle \omega_x^2 u \right\rangle$, dotted line:$-\frac{1}{2}\left\langle \omega_y^2 u \right\rangle$, dash-dotted line$-\frac{1}{2}\left\langle \omega_z^2 u \right\rangle$. t/t_0= 8.6 .

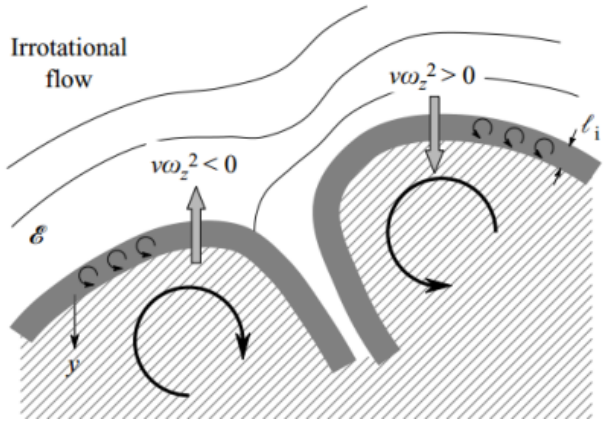

Figure 2.3.18: Example of the contribution of the vorticity component ω_z at the interface (Westerweel 2009)

$-\frac{1}{2}\left\langle \omega_y^2 u \right\rangle$ have both skewed narrow profiles, see figure 2.3.19 (right). The longitudinal variation shows that the pdf start from having a symmetrical profile in the turbulent core, and lose the symmetry in the interface, i.e. a mean value is reached.

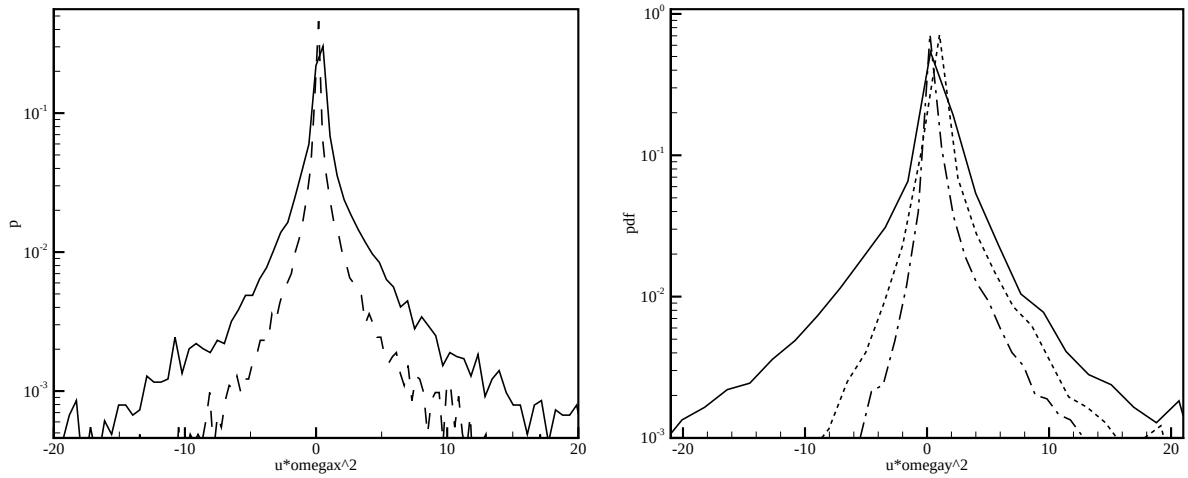

Figure 2.3.19: (Left) Probability density function for $-\frac{1}{2}\left\langle \omega_x^2 u \right\rangle$. (Right) $-\frac{1}{2}\left\langle \omega_y^2 u \right\rangle$ at different longitudinal positions. Solid line: turbulent core, dashed line: turbulent interface, dash-dotted: x=0.5 . t/t_0= 8.6.

Moreover the skewness of the longitudinal component at the interface is much less demarcated respect the transverse one. Hence it seems from these data that the inertial transport of vorticity toward the interface plays a fundamental role, refurnishing the interface with new vorticity to be dissipated in the entrainment process.
The viscous diffusion of turbulence instead gets its relevance on the interface surface. This mechanism is strongly affected by the extension of the exposed surface of the turbulent front and on the local Reynolds number. An assessment of the total interface area has been done by Sreenivasan et al. (1989). In his work the surface of the interface is modeled with a fractal three dimensional surface. The smallest structure length of this fractal surface, called inner cut-off lengthr_i, is assumed to be the Kolmogorov scale η.The area S_T of such surface with finite inner cut-off is given by

$$S_T = S_0 \left(\frac{r_i}{L}\right)^{2-d} \tag{2.3.14}$$

where S_0 is an estimate of the interface utilizing an arbitrary length L. The parameter L

has been taken as the domain widht π, hence the surface S_0 is π^2. The parameter d is the fractal dimension of the surface and for mixing layers is reported to be 7/3. Being the fractal surface proportional to $\eta^{-1/3}$, it decays with the increase of η with time. In fact the total surface predicted for the considered time range decrease from 41.9 to 37.7. These values gives an estimate on the surface contraction due to the erosion of the small scales, which indirectly affect the viscous flux of turbulence; the decay of such flux can be seen in figure 2.3.20.

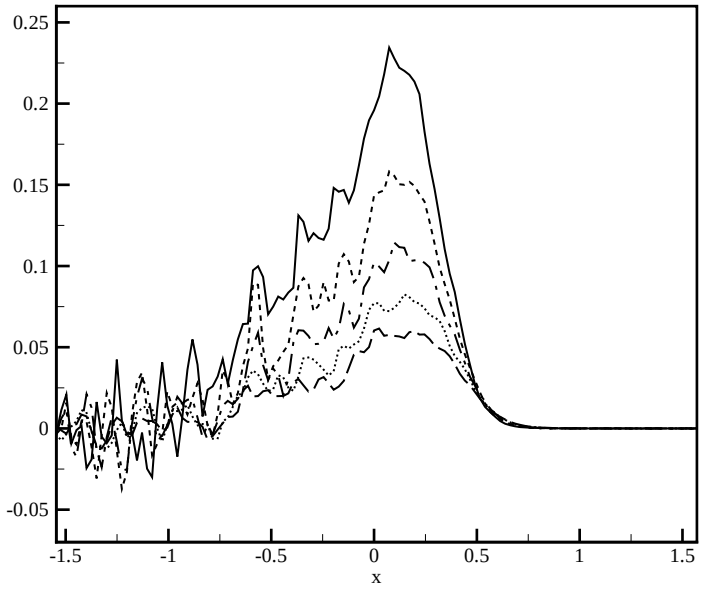

Figure 2.3.20: Time evolution of the viscous flux. Time steps from t/t_0=5.2 (highest level) to 8.6.

The smallest resolved structure in the simulation is $r_{min} = 2\pi/128 = 0.049$, hence the ratio between the theoretical fractal surface S_T and the resolved fractal surface S_R is

$$\frac{S_T}{S_R} = \left(\frac{\eta}{r_{min}}\right)^{2-d} = \left(\frac{\eta}{0.049}\right)^{-\frac{1}{3}} \tag{2.3.15}$$

In the range of temporal iterations we have considered in this work the Kolmogorov length η grows from 0.041 to 0.056, against a spatial resolution of 0.049, hence the maximum error in estimating the interface surface is about the 6% for t/t_0=5.2.
In order to better asses some aspects of enstrophy evolution, it is interesting to extend

the study of enstrophy balance equation to Fourier space. An hybrid formulation in the the variables $x-k_y-k_z$ will be used due to the inhomogeneity of the flow in the x direction. Thus we report now the formulation of the hybrid spatial-spectral version of the enstrophy balance equation . Starting from the equation of vorticity

$$\frac{\partial \omega_i}{\partial t} + u_j \frac{\partial \omega_i}{\partial x_j} = \omega_j \frac{\partial u_i}{\partial x_j} + \nu \frac{\partial^2 \omega_i}{\partial x_j \partial x_j}. \tag{2.3.16}$$

Transforming in the Fourier space the equation above we obtain

$$\frac{\partial \hat{\omega}_i}{\partial t} + u_j \widehat{\frac{\partial}{\partial x_j} \omega_i} = \omega_j \widehat{\frac{\partial u_i}{\partial x_j}} - \nu k^2 \hat{\omega}_i, \tag{2.3.17}$$

where $k^2 = k_x^2 + k_y^2 + k_z^2$. The relation above can be rewritten as

$$\frac{\partial \hat{\omega}_i}{\partial t} + ik_j \widehat{u_j \omega_i} = ik_j \widehat{\omega_j u_i} - \nu k^2 \hat{\omega}_i. \tag{2.3.18}$$

We multiply now the 2.3.17 by the complex conjugate of $\hat{\omega}_i$ and we expand its second term

$$\frac{1}{2} \frac{\partial}{\partial t} \hat{\omega}_i \hat{\omega}_i^* + \hat{\omega}_i^* \widehat{\frac{\partial}{\partial x_j} \omega_i u_j} = \hat{\omega}_i^* \omega_j \widehat{\frac{\partial u_i}{\partial x_j}} - \nu k^2 \hat{\omega}_i \hat{\omega}_i^*. \tag{2.3.19}$$

The terms of this equation are in the Fourier space but we look for an equation that is in the Fourier space in the y and z directions and in the physical space in the x direction. In order to do so we transform back the terms in equation 2.3.19 only in the variable x. We will indicate the derivatives in the Fourier plane $k_y - k_z$ as $k_\pi = k_y^2 + k_z^2$ and the hybrid transform operation as $\sim$, for example the hybrid vorticity field will be $\tilde{\omega} = \omega(x, k_y, k_z)$. The result lead to

$$\frac{1}{2} \frac{\partial}{\partial t} \tilde{\omega}_i \tilde{\omega}_i^* + ik_\pi \tilde{\omega}_i^* \widetilde{\omega_i u_\pi} + \tilde{\omega}_i^* \frac{\partial}{\partial x} \widetilde{\omega_i u_j} = \tilde{\omega}_i^* \omega_j \widetilde{\frac{\partial u_i}{\partial x_j}} - \nu k_\pi^2 \tilde{\omega}_i \tilde{\omega}_i^* + \nu \tilde{\omega}_i^* \frac{\partial^2}{\partial x^2} \tilde{\omega}_i, \tag{2.3.20}$$

finally the last term of the equation is expanded, obtaining

$$\frac{1}{2} \frac{\partial}{\partial t} \tilde{\omega}_i \tilde{\omega}_i^* + ik_\pi \tilde{\omega}_i^* \widetilde{\omega_i u_\pi} + \tilde{\omega}_i^* \frac{\partial}{\partial x} \widetilde{\omega_i u_j} = \tilde{\omega}_i^* \omega_j \widetilde{\frac{\partial u_i}{\partial x_j}} - \nu k_\pi^2 \tilde{\omega}_i \tilde{\omega}_i^* + \frac{\nu}{2} \frac{\partial^2}{\partial x^2} \tilde{\omega}_i \tilde{\omega}_i^* - \nu \frac{\partial \tilde{\omega}_i}{\partial x} \frac{\partial \tilde{\omega}_i^*}{\partial x} \tag{2.3.21}$$

The complete analysis of all the term of the spectral balance equation will be addressed in future studies, but we report as example the results for the term $-\nu k_\pi^2 \tilde{\omega}_i \tilde{\omega}_i^*$. The plot of the term $-\nu k_\pi^2 \tilde{\omega}_i \tilde{\omega}_i^*$ is reported in figure 2.3.21. It represents the component of viscous dissipation of vorticity due to the fluctuations in the homogeneous space k_π^2. The plot highlights that as expected the dissipation reaches its maximum at small scales. The wave number around which $\nu k_\pi^2 \tilde{\omega}_i \tilde{\omega}_i^*$ reaches its maximum seems to be independent with respect to the spatial position, consistently whit the behavior seen in the plot of Ω_k where all the scales are observed to decrease in space with the same rate.

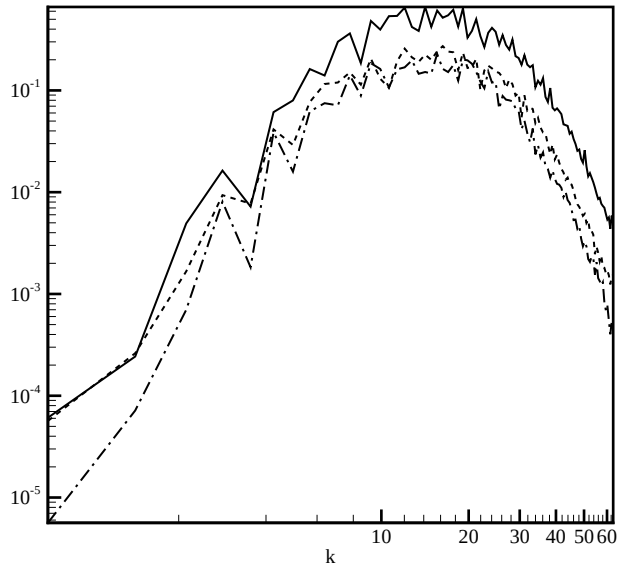

Figure 2.3.21: Absolute value of the spectrum of $-\nu k_\pi^2 \tilde{\omega}_i \tilde{\omega}_i^*$Solid line: turbulent core, dashed: interface , dash-dotted: x= 1.6

2.3.5 Strain rates

Strain must be addressed in our analysis since it plays an essential role in turbulence. Dissipation is directly associated with strain rates through the relation $\epsilon = 2\nu s_{ij} s_{ij}$. Vortex stretching, one of the main mechanism of vorticity amplifications, involves the interaction between vorticity and strain. Furthermore, it is thought that the energy cascade and dissi-

pation, are associated with predominant self-amplification of the rate of strain/production and vortex compression rather than with vortex stretching (Tsinober 2001).
Vorticity and strain are strongly related, they are derivatives of the same velocity fields and without vorticity there is no strain production. There are then many relation between the enstrophy field and the strain field.

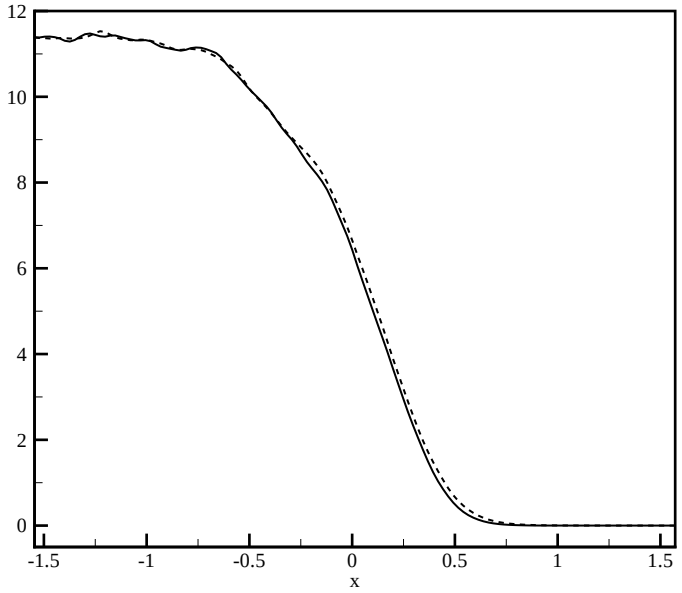

Comparison between enstrophy $\frac{\omega^2}{2}$ (solid line) and strain s^2(dashed). t/t_0=8.6 .

In the turbulent side of the flow, strain and enstrophy have similar values due to the fact that the flow here can be approximate as isotropic. and homogeneous. Indeed, from the definition of enstrophy and strain we have

$$\frac{\langle\omega^2\rangle}{2} = \left\langle \frac{\partial u_i}{\partial x_j}\frac{\partial u_i}{\partial x_j} \right\rangle - \left\langle \frac{\partial u_i}{\partial x_j}\frac{\partial u_j}{\partial x_i} \right\rangle \tag{2.3.22}$$

$$\langle s_{ij}^2\rangle = \left\langle \frac{\partial u_i}{\partial x_j}\frac{\partial u_i}{\partial x_j} \right\rangle + \left\langle \frac{\partial u_i}{\partial x_j}\frac{\partial u_j}{\partial x_i} \right\rangle, \tag{2.3.23}$$

which can be rewritten as

$$\frac{\langle\omega^2\rangle}{2} = \frac{1}{2}\left\langle \frac{\partial u_i}{\partial x_j}\frac{\partial u_i}{\partial x_j} \right\rangle - \frac{1}{2}\frac{\partial}{\partial x_i}\left\langle \frac{\partial}{\partial x_j}u_i u_j \right\rangle \tag{2.3.24}$$

$$\left\langle s_{ij}^2 \right\rangle = \frac{1}{2}\left\langle \frac{\partial u_i}{\partial x_j}\frac{\partial u_i}{\partial x_j} \right\rangle + \frac{1}{2}\frac{\partial}{\partial x_i}\left\langle \frac{\partial}{\partial x_j} u_i u_j \right\rangle . \tag{2.3.25}$$

Hence in the homogeneous part of the flow the second term of both strain and enstrophy is zero, and we have

$$\frac{\left\langle \omega_i^2 \right\rangle}{2} = \left\langle s_{ij}^2 \right\rangle = \frac{\epsilon}{2\nu} \tag{2.3.26}$$

However, as shown in figure 2.3.5, in correspondence of the interface these two terms slightly deviate. Indeed, due to the inhomogeneity induced by the presence of the interface, the second term of equations 2.3.22 and 2.3.23 is not zero, hence

$$\frac{\left\langle \omega^2 \right\rangle}{2} - \left\langle s_{ij}^2 \right\rangle = -\left\langle \frac{\partial u_i}{\partial x_j}\frac{\partial u_j}{\partial x_i} \right\rangle \tag{2.3.27}$$

When inhomogeneity grows the cross-gradient term is non-zero and the local enstrophy differ from the strain by $\frac{\partial}{\partial x_i}\left\langle \frac{\partial}{\partial x_j} u_i u_j \right\rangle$; this term become relevant in the part of the field where enstrophy start to decrease. The departure of strain from enstrophy in the turbulent flow start about at the same ordinate of the peak of inertial flux.
The variation of the strain at a given time is

$$\frac{d}{dt}\frac{s^2}{2} = -s_{ij}s_{jk}s_{ki} - \frac{1}{4}\omega_i\omega_j s_{ij} - s_{ij}\frac{\partial^2 p}{\partial x_i \partial x_j} + \nu s_{ij}\nabla^2 s_{ij}, \tag{2.3.28}$$

as did before for enstrophy balance equation, this equation can be decomposed as

$$\frac{\partial}{\partial t}\frac{\left\langle s^2 \right\rangle}{2} = -\frac{1}{2}\frac{\partial}{\partial x}\left\langle s_{ij}^2 u \right\rangle - \left\langle s_{ij}s_{ik}s_{ki} \right\rangle - \frac{1}{4}\left\langle \omega_i\omega_j s_{ij} \right\rangle - \left\langle s_{ij}\frac{\partial^2 p}{\partial x_i \partial x_j} \right\rangle + \frac{\nu}{2}\frac{\partial^2}{\partial x^2}\left\langle s_{ij}^2 \right\rangle - \nu\left\langle \frac{\partial s_i}{\partial x_j}\frac{\partial s_i}{\partial x_j} \right\rangle . \tag{2.3.29}$$

Once again the first term is the inertial transport and the last two term represent viscous diffusion of strain and viscous dissipation. The triple correlation term $-\left\langle s_{ij}s_{ik}s_{ki} \right\rangle$ is responsible for strain production, while $-\left\langle s_{ij}\frac{\partial^2 p}{\partial x_i \partial x_j} \right\rangle$ is the term of interaction between strain and pressure gradients.
The behavior of the terms of the strain rate balance equation is similar in many aspect to the behavior of their "equivalent" terms of enstrophy balance equation. There is in fact a strong negative variation of strain in the turbulent core due to both viscous dissipation and the interactions with the vorticity field (figure 2.3.22) . These are counteracted by the

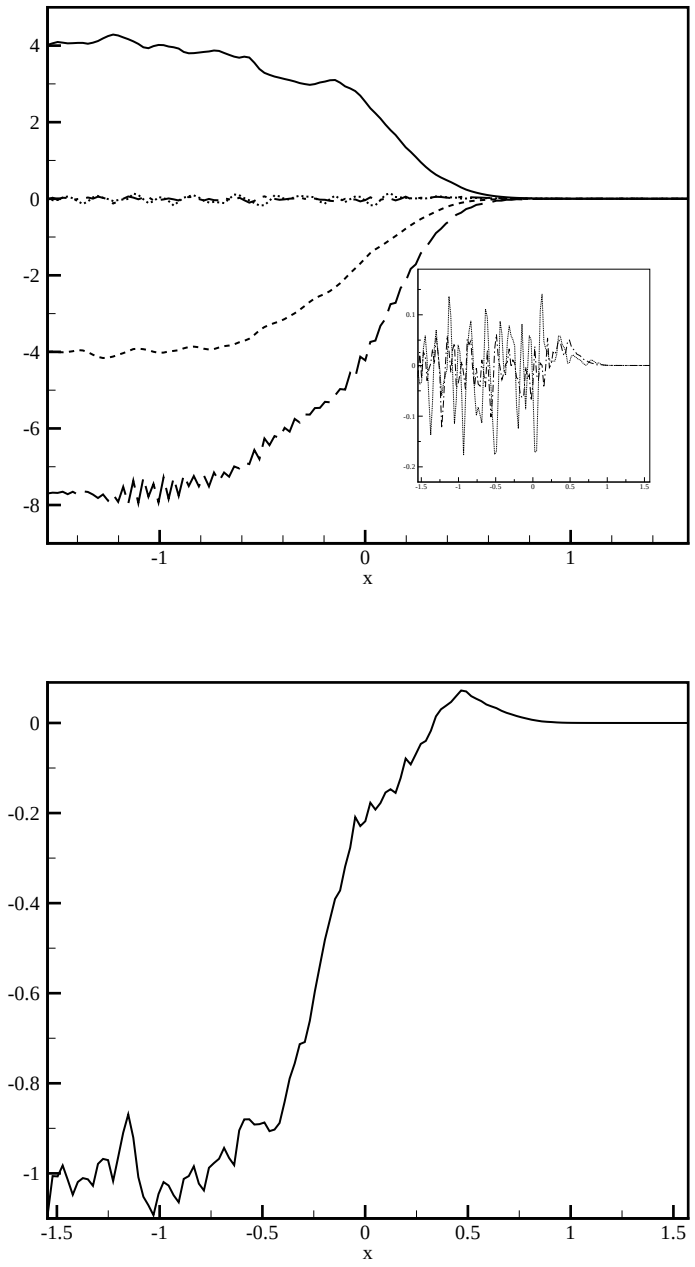

Figure 2.3.22: (Above) Components of strain balance at t/t_0 = 8.6. Solid line: $-\left\langle s_{ij}s_{ik}s_{ki}\right\rangle$, dashed line: $-\frac{1}{4}\left\langle \omega_i\omega_j s_{ij}\right\rangle$, long dashed: $-\nu\left\langle \frac{\partial s_i}{\partial x_j}\frac{\partial s_i}{\partial x_j}\right\rangle$, dash-dot: $\frac{\nu}{2}\frac{\partial^2}{\partial x^2}\left\langle s_{ij}^2\right\rangle$, dotted line: $-\frac{1}{2}\frac{\partial}{\partial x}\left\langle s_{ij}^2 u\right\rangle$. (under) The sum of the four terms above.

triple correlation term and the two diffusive terms, the first being some order of magnitude stronger than diffusive terms. Inertial and viscous diffusion become significant near the interface, though the inertial transport relevance found for vorticity is not present for the strain rate. The sum of these terms can be seen in the bottom of figure 2.3.22, similarly to the enstrophy balance equation, a peak of positive variation of strain rate can be found.

2.3.6 Some considerations on interface detection

In order to visualize the turbulent interface, the threshold technique has been choesen. As mentioned in chapter 1.3.2 this technique marks the points at which an arbitrary value of enstrophy or kinetic energy is reached. The Lagrangian analysis of the entrainment seems to justify such approach: Holzner et al. (2008) found in both PIV measurement and DNS that effectively, on the average, the particles which cross the interface toward the turbulent flow experience a sharp rise in esntrophy and kinetic energy (and other properties such the strain rate).
In the present work, the threshold method has been proven successful in providing a continuous and "smooth" surface for the turbulent front (see figure 2.3.23). It has been applied also to the normalized profiles of both energy and enstrophy (figure 2.3.24) in order to find the average position of the interface. The kinetic and enstrophy profiles normalized with their respective maxima, highlights an advancement of the front with time. Indeed as shown in figure 2.3.25, it is possible to track the position of the interface in time. From the plot it appears that the interface moves toward the laminar region proportionally to $t^{1/2}$.This highlights how the progression of the interface is strongly related with viscous diffusion,from which dimensional analysis gives $L_{diff} \sim \sqrt{\nu t}$.
The variation of the threshold level strongly affect the results, this is particularly valid for the application to small Reynolds numbers flows, but also high Reynolds flows are affected by such issue. Jimenez addressed (2012) the problem in boundary layers interfaces and stated that, for a vorticity jump of about two order of magnitude respect the residual vorticity in the non turbulent flow, the range of eligible threshold values is still almost one order of magnitude. In this range the topology of structures that can be encountered variate significantly; as can be seen in figure 2.3.23, with the variation of threshold, the interface start as a smooth uniform surface at low values and became a convoluted assemble of structures and bubbles of vorticity at higher ones. As in the boundary layer case, this

change is visible in a range of less than an order of magnitude and in such range the estimate of interface position and its estimated surface change sensibly.
By utilizing an absolute value for the threshold on the non-normalized profiles (i.e. not a percentage of the turbulent core values), a much different behavior can be observed, the interface position appears to reach a maximum after which it starts to go back (figure 2.3.25 right). As third approach, the position of the maximum of enstrophy variation $\frac{\partial}{\partial t}\omega^2$ has been evaluated. This shown a linear advancement not found in any other quantity (figure 2.3.14).

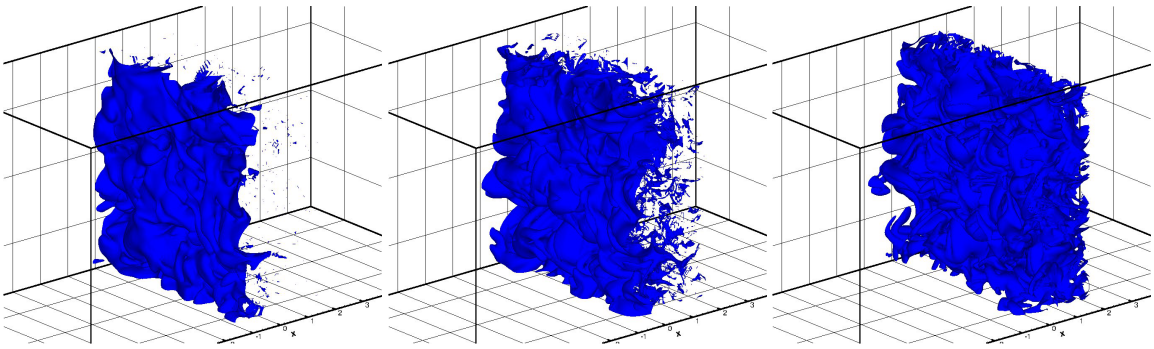

Figure 2.3.23: Variation of the iso-surface of enstrophy with the threshold: left 1%, center 10%, right 90%

The detection technique must be addressed accurately, since the estimate position of the interface has often been used for the computation of conditioned statistics and for the analysis of small scales mechanics across the interface. The risk is the one of filter out some phenomena which are undergoing far from the estimated turbulent interface, but which equally contributes in the entrainment process.
In this work has been found that the interface in decaying turbulence manifest a stratified phenomenology on a spread range, thus an interface definition which comprehend all such range is hard to find. The inertial flux, for example, become significant in the turbulent flow before the threshold detected interface and it appears to be almost static, thus independent respect the detected interface position. The viscous flux has a similar independence, but with a position which is slightly before the range of interface position found with a 10% thresholds. On the other hand the position of the maximum of enstrophy balance falls well beyond any threshold detected interface, leaving it virtually outside the entrainment phenomenology. It must be noted that the case study analyzed here is peculiar: the turbulence

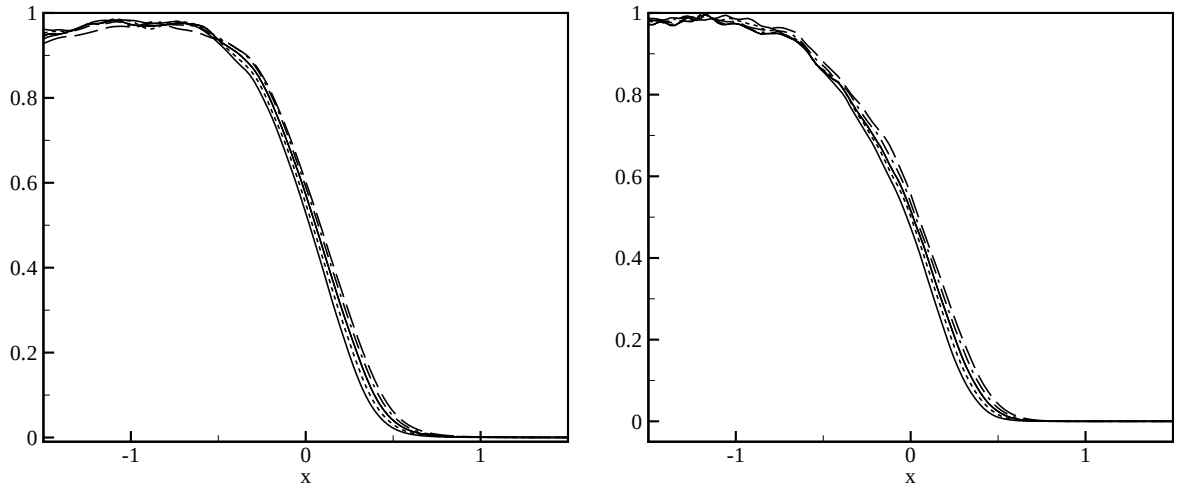

Figure 2.3.24: (Right) Kinetic energy and (left) enstrophy profiles normalized by their respective maxima. Solid: t/t_0=5.2 , dashed: 6.0 , dotted: 6.9,dash-dotted: 7.8 ,long dashed: 8.6

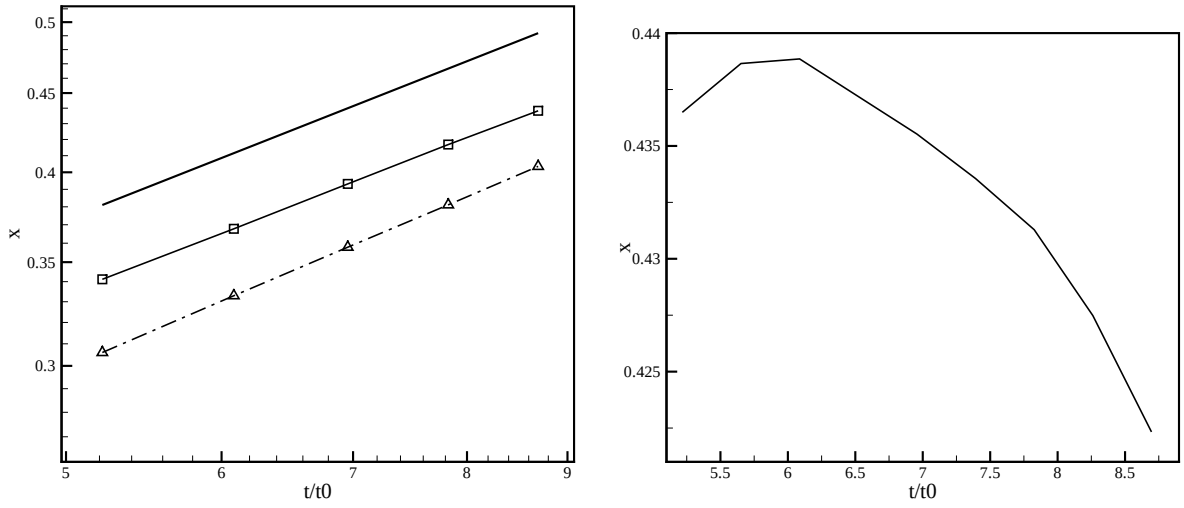

Figure 2.3.25: (Left) Position of the 10% threshold of enstrophy and kinetic energy (respectively $\frac{\omega^2}{\omega^2_{max}}$ (dot-dashed) and $\frac{E_k}{E_{k_{max}}}$ (solid)). The solid thick line represent $t^{\frac{1}{2}}$. (Right) The same position detected with a fixed threshold $\omega^2_{th} = \frac{1}{10}\omega^2_{max}(t = 8.6)$

is not sustained by any external energy injection, therefore the vorticity ranges become rapidly particularly small.

Conclusion

A shearless turbulent/non-turublent interface was studied in the framework of a decaying turbulence; such flow has been simulated with a high accuracy DNS pseudo-spectral code. A turbulent field constituted by two interfaces has been "artificiously" generated from a core of initially homogeneous isotropic turbulence; the resulting field has been let freely evolve without forcing. Though the flow cannot be reproduced in an actual experiment, it has many similarities with previous experiments conduced on turbulence generated by oscillating grids (Holzner et al. 2007). The evolution of this turbulence has been studied through its spatial and temporal variations, with special focus on enstrophy and enstrophy production. Velocity fluctuations and vorticity across the interface, shown the characteristic steep profiles already observed in previous works on turbulent/non-turbulent interface (Westerweel 2009, Holzner 2007, Liberzon 2009). The decay rate of the isotropic homogeneous core of the field, as expected, has been found greater then the homogeneous case without the interface, but it still follows a power law decay. The decay rate in the rest of the field is dependent respect the inhomogeneous direction, but it appears to follow a power law decay also at the interface.

The measurements of enstrophy evidence a zone of positive variation ($\frac{\partial}{\partial t}\omega^2 > 0$), which denotes the undergoing entrainment process; outside this limited range, the vorticity dissipation always prevails in the turbulent flow. The analysis of the enstrophy balance equation terms shows that such positive variation of enstrophy is locally determined by the contribute of three quantities that counteract the viscous dissipation, $-\nu\frac{\partial\omega_i}{\partial x_j}\frac{\partial\omega_i}{\partial x_j}$. These are the local production term $\omega_i\omega_j s_{ij}$ which is the consequence of inviscid interactions between the vorticity and the strain fields, the viscous diffusion of turbulence $\frac{\nu}{2}\frac{\partial^2}{\partial x_j}\omega_i^2$ and the inertial transport of turbulence $-\frac{1}{2}\frac{\partial}{\partial x_j}u_j\omega_i^2$.

The data produced has shown that for a shearless interface of decaying turbulence, the inertial transport of vorticity has a bigger role than expected for the enstrophy balance in

proximity of the interface. This does not agree with the measurement in previous work (Westerweel et al. 2009) and it is still unclear if it is due to the differences in the two type of flows.

Different threshold techniques for interface detection have been evaluated. By using a fixed percentage threshold of enstrophy we have been able to detect a propagation of the interface toward the laminar region which follows a square-root behavior in time ($\sim \sqrt{t}$), in agreement with a viscous process. Whereas, by using the maxima of enstrophy variation, $\frac{\partial}{\partial t}\omega^2 > 0$, we found a linear propagation of the interface in time. These two trend highlights the dependence of the results on the interface detection technique.

Future studies will analyze the spectral enstrophy budget equation, here introduced in order to address the role of the spatial fluxes on the injection of large scales fluctuations into irrotational flow with respect the small scale dissipation in such region. Interesting will be also the extension of the analysis of the present work to forced turbulence where the equilibrium between dissipation and production of vorticity is reached. Such flow would permit to better analyze the dynamics of propagation velocity and entrainment rate. Further studies will address the turbulent/non-turbulent interface behavior in flow with shear. This feature belongs to more realistic flows such as boundary layers, jets and wakes.

Bibliography

[1] J.D. Anderson. *Computational fluid dynamics, the basics with applications*. McGraw-Hill Science, 1995.

[2] E. De Angelis, C.M. Casciola, R. Benzi, and R. Piva. Homogeneous isotropic turbulence in dilute polymers. *J. Fluid Mech.*, 2005.

[3] D.K. Bisset, J.C.R. Hunt, and M.M. Rogers. The turbulent/non-turbulent interface bounding a far wake. *J. Fluid Mech.*, 2001.

[4] G. Borrell and J. Jimenez. The geometry of the entrophy interface in boundary layers, 2012. excerpt from the Multiflow workshop on the turbulent/nonturbulent interface, Madrid.

[5] G. Comte-Bellot and S. Corrsin. The use of a contraction to improve the isotropy of grid-generated turbulence. *J. Fluid Mech.*, 1966.

[6] S. Corrsin. Investigation of flow in an axially symmetric heated jet in air. *NACA ACR 3L23*, 1943.

[7] K. George. *Lectures in turbulence for the 21st century*. 2013. lecture notes.

[8] M. Holtzner, A. Liberzon, B. Luthi, W. Kinzelbach, and A. Tsinober. The local entrainment velocity is a viscous quantity. *Turbulence, Heat and Mass Transfer 6*, 2009.

[9] M. Holtzner, A. Liberzon, N. Nitkin, B. Luthi, W. Kinzelbach, and A. Tsinober. A lagrangian investigation of the small-scale features of turbulent entrainment through particle tracking and direct numerical simulation, 2007. J. Fluid Mech.

[10] M. Holtzner, A. Liberzon, N. Nitkin, B. Luthi, W. Kinzelbach, and A. Tsinober. Small scales aspects of flows in proximity of the turbulent/non-turbulent interface, 2007. Phys. Fluids.

[11] M. Holtzner, B. Luthi, A. Tsinober, and W. Kinzelbach. Acceleration, pressure and related quantities in the proximity of the turbulent/ non-turbulent interface, 2009. J. Fluid Mech.

[12] J. Scott J. Mathieu. *An introduction to turbulent flow*. Cambridge University Press, 2000.

[13] A. Liberzon, M. Holzner, B. Luthi, M. Guala, and W. Kinzelbach. On turbulent entrainment and dissipation in dilute polymer solutions. *Phys. Fluids*, 2009.

[14] R.R. Long. Theory of turbulence in a homogeneous fluid induced by an oscillating grid, 1978. Phys. Fluids.

[15] L. Hesselink M. Yoda and M. G. Mungal. The evolution and nature of largescale structures in the turbulent jet. *Phys. Fluids*, 1991.

[16] O. Obliquy. Pseudo-spectral methods apllied to hydrodynamic and magnetohydrodynamic turbulence., 2004. PhD. Thesis, Unversite' libre de Bruxelles, Faculte' des Sciences.

[17] J.C. Vassilicos P.C. Valente. The decay of turbulence generated by a class of multiscale grids. *J. Fluid Mech.*, 2011.

[18] J. Philip, K. Chauhan, and I. Marusic. Turbulent/non-turbulent interface and entrainment in shera flows, 2012. excerpt from the Multiflow workshop on the turbulent/nonturbulent interface, Madrid.

[19] S.B. Pope. *Turbulent flows*. Cambridge University Press, 2000.

[20] M. Quadrio. Turbolenza: dispense del corso, 2012. Politecnico di Milano.

[21] A.L. Kistler S. Corrsin. The free-stream boundaries of turbulent flows. *NACA TN-3133, TR-1244*, 1955.

[22] P. Schlatter. Spectral methods. notes for Computational fluid dynamics SG2212.

[23] R.E. Seud and J.C. Vassilicos. Dissipation and decay of fractal-generated turbulence. *Phys. Fluids*, 2007.

[24] K.R. Sreenivasan, R. Ramshankar, and C. Menevau. Mixing, entrainment and fractal dimensions of surfaces in turbulent flows. *Proc. R. Soc. Lond.*, 1989.

[25] R.R. Taveira and C.B. da Silva. Aspects of the turbulent/non-turbulent interface for the velocity field, 2012. excerpt from the Multiflow workshop on the turbulent/nonturbulent interface, Madrid.

[26] D. Tordella, M. Iovieno, and P.R. Bailey. Sufficient condition for gaussian departure in turbulence. *Phys. Rev. E.*, 2008.

[27] D.J. Tritton. *Physical Fluid Dynamics, second edition*. Oxford Science Publications, 1988.

[28] A. Tsinober. *An informal introduction to turbulence*. Kluwer Academic Publishers, 2001.

[29] J. Westerweel, C. Fukushima, Jakob Martin Pedersen, and J. C. R. Hunt. Momentum and scalar transport at the turbulent/non-turbulent interface of a jet. *Journal of Fluid Mechanics*, 2009.

[30] J. Westerweel, C. Fukushima, J.M. Pedersen, and J.C.R. Hunt. Mechanics of the turbulent-nonturbulent interface of a jet. *Phys. Rev. Lett.*, 2005.